Journal of Asian Earth Sciences 192 (2020) 104236

Contents lists available at ScienceDirect

Journal of Asian Earth Sciences

journal homepage: www.elsevier.com/locate/jseaes

Petrogenesis of Late Jurassic Pb–Zn mineralized high $\delta^{18}O$ granodiorites in the western Nanling Range, South China

Xiao Liu[a,b], Qiang Wang[a,b,c,*], Lin Ma (PhD)[a,*], Derek A. Wyman[d], Zhen-Hua Zhao[e], Jin-Hui Yang[f], Feng Zi[g], Gong-Jian Tang[a,c], Wei Dan[a,c], Jin-Sheng Zhou[a]

[a] State Key Laboratory of Isotope Geochemistry, Guangzhou Institute of Geochemistry, Chinese Academy of Sciences, Guangzhou 510640, China
[b] College of Earth and Planetary Sciences, University of Chinese Academy of Sciences, Beijing 100049, China
[c] CAS Center for Excellence in Tibetan Plateau Earth Sciences, Beijing 100101, China
[d] School of Geosciences, University of Sydney, New South Wales 2006, Australia
[e] Key Laboratory of Mineralogy and Metallogeny, Guangzhou Institute of Geochemistry, Chinese Academy of Sciences, Guangzhou 510640, China
[f] Institute of Geology and Geophysics, Chinese Academy of Sciences, Beijing 100029, China
[g] School of Resource & Environment and Safety Engineering, Hunan University of Sciences and Technology, Xiangtan 411201, China

ARTICLE INFO

Keywords:
Amphibole-bearing granite
Partial melting of metasedimentary and metaigneous rocks
Western Nanling Range
South China

ABSTRACT

Amphibole-bearing granites are commonly considered to be I-type granites, derived by partial melting of igneous rocks. However, the contribution of sedimentary rocks to the source of such rocks is difficult to identify and remains debated. Here, we present a study of amphibole-bearing Pb-Zn mineralized granodiorites in the western Nanling Range of South China. LA–ICP–MS zircon U–Pb ages show that these granodiorites were generated during the Late Jurassic (ca. 161 Ma). They have variable SiO_2 contents of 61.8–70.7 wt% and have high-K or shoshonitic characteristics, with varied $Mg^{\#}$ (0.28–0.54). These granodiorites are enriched in Th and U, and depleted in Nb, Ta and Ti. They display enriched light rare earth element (LREE) and flat heavy rare earth element (HREE) patterns, with slightly negative to negligible Eu anomalies (δEu = 0.74–0.95). Given their high zircon $\delta^{18}O$ values (8.8‰–11.9‰), as well as negative $\varepsilon_{Nd}(t)$ (−7.5 to −5.1) and zircon $\varepsilon_{Hf}(t)$ (−13.9 to −7.5) values, we suggest that these Pb-Zn mineralized granodiorites in the western Nanling Range were derived mainly by partial melting of Middle Neoproterozoic mafic volcaniclastic rocks from the Nanhua rift basin, South China, in the lower crust. This study provides an important insight into the genesis of amphibole-bearing granites. We suggest that the partial melting of crustal metasedimentary and metaigneous rocks is an important mechanism for the Mesozoic crustal reworking of South China, and granodiorites generated by such a mechanism should also favor Pb–Zn mineralization.

1. Introduction

Granite is one of the most important components of the upper continental crust, which makes Earth distinct from the other planets in the Solar System (Wu et al., 2007a). Given that granitic magmas play a critical role in the geochemical differentiation of continental crust (Gao et al., 2016), they have been the subject of intensive research for many decades. The most widely used genetic classification, into I-type and S-type granites, was proposed by Chappell and White (1974) on the basis of granitoid studies in the Lachlan Fold Belt, Australia. Generally, amphibole and cordierite are considered to be the diagnostic minerals of I-type and S-type granites, respectively (Chappell and White, 1974, 2001). Comprehensive experimental petrology studies suggest that amphibole- and biotite-bearing basaltic and andesitic igneous arc rocks are the source of I-type granites (Gao et al., 2016, and references therein). However, it is debated whether a substantial sedimentary rock is present in the source of typical amphibole-bearing I-type granites (Kemp et al., 2007; Huang et al., 2015a; Wang et al., 2018). Identifying the contribution of sedimentary rocks to the formation of such I-type granites remains an unsolved problem. Here we use the Late Jurassic amphibole-bearing granodiorites from South China to address this issue.

Mesozoic granitoids are widely distributed in South China and the area of outcrop of these Mesozoic granitoids is ~135,300 km^2 (He et al., 2010). There is a general consensus that the petrogenesis of these granitoids involved reworking of significant crustal material (Jiang

* Corresponding authors at: State Key Laboratory of Isotope Geochemistry, Guangzhou Institute of Geochemistry, Chinese Academy of Sciences, Guangzhou 510640, China.
E-mail addresses: wqiang@gig.ac.cn (Q. Wang), malin@gig.ac.cn (L. Ma).

https://doi.org/10.1016/j.jseaes.2020.104236
Received 25 July 2019; Received in revised form 6 January 2020; Accepted 8 January 2020
Available online 31 January 2020
1367-9120/

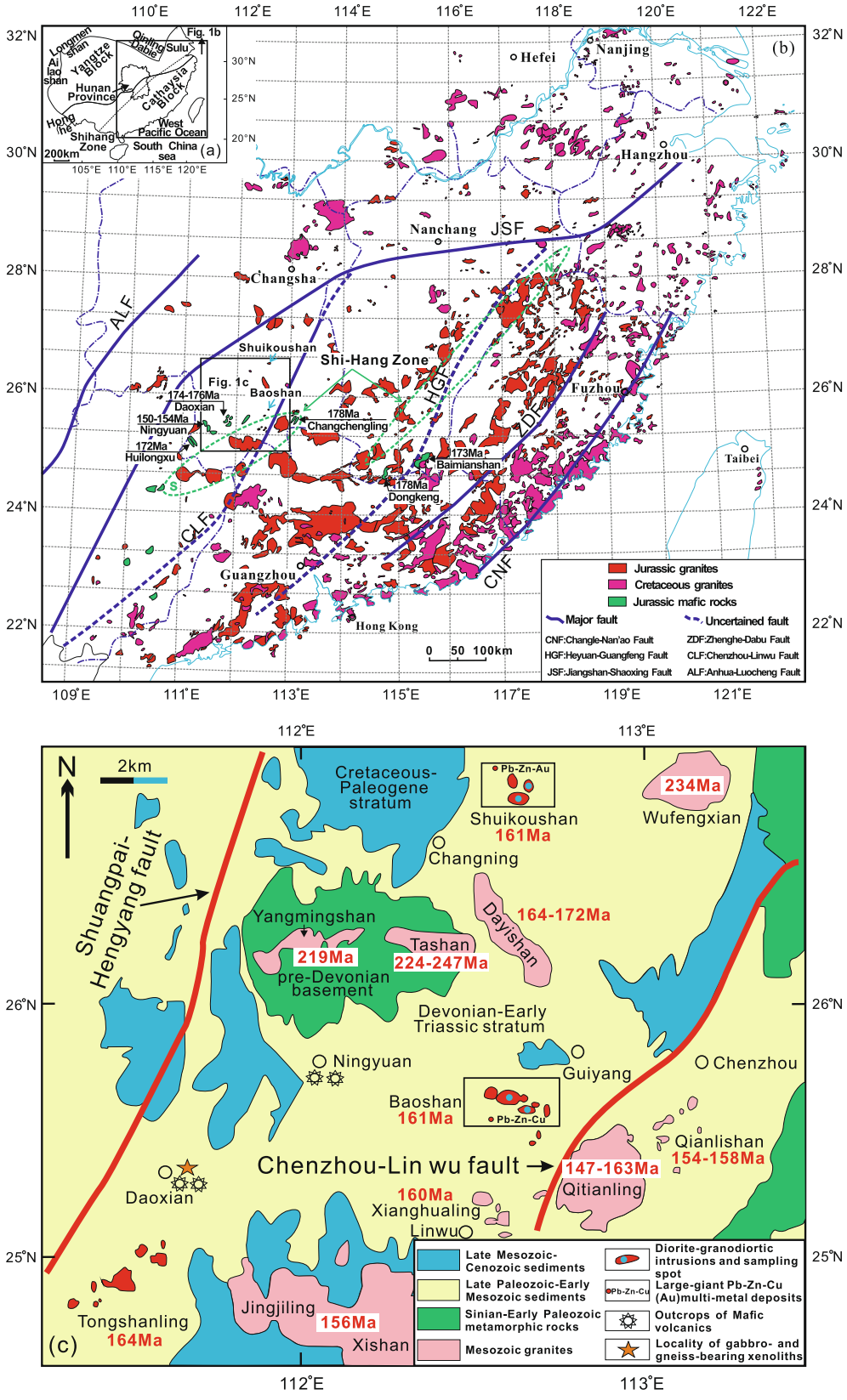

Fig. 1. (a) Simplified regional map highlighting the tectonic framework of the SCB, composed of the Yangtze and Cathaysia blocks (modified from Zheng et al., 2007). (b) Sketch map showing the location of Jurassic and Cretaceous granitic and Jurassic mafic rocks in the SCB (modified from Sun, 2006; Yang et al., 2016). Age data are from Wang et al. (2003b, 2008b). (c) Simplified geological map of the Shuikoushan and Baoshan granodiorites in the western Nanling Range (modified from Wang et al., 2003a), showing rock types and sample locations. The ages of Mesozoic granites in the western Nanling Range are from this study (Shuikoushan and Baoshan); Qiu et al. (2003) (Xianghualing); Jiang et al. (2009), and references therein (Jinjiling–Xishan and Tongshanling); Li et al. (2015), and references therein (Dayishan, Tashan, Qitianling, and Yangmingshan); Chen et al. (2016) (Qianlishan); and Chen et al. (2017) (Wufengxian).

et al., 2009; Shu et al., 2011), and the South China Block (SCB) likely experienced significant Mesozoic continental reworking (e.g. Xu et al., 2007). In particular, the Jurassic was a significant period of magmatic activity and metal ore formation in South China (Huang et al., 2015b). Numerous Jurassic Pb–Zn–Cu and W–Sn–Nb–Ta mineral deposits are closely related, both temporally and spatially, to Jurassic granitoids (Huang et al., 2015b). Jurassic magmatism in South China occurred mainly between 180 and 140 Ma (Zhou et al., 2006; Li et al., 2007). Jurassic amphibole-bearing granites are mainly exposed in the western Nanling Range, in the center part of the SCB (Fig. 1a), such as the

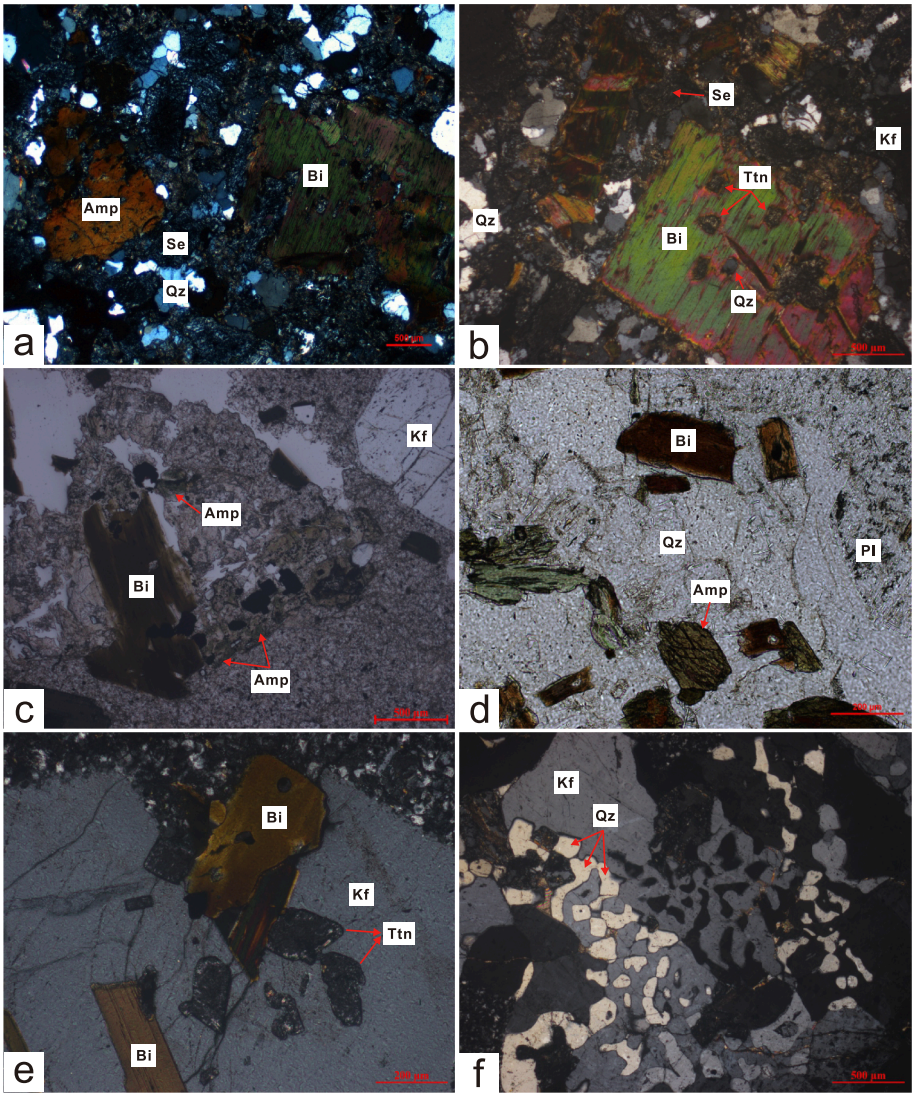

Fig. 2. Photomicrographs of the Shuikoushan and Baoshan plutons, showing (a–b) the Shuikoushan granodiorite, and (c–f) the Baoshan granodiorite. Mineral abbreviations: Qz = quartz; Amp = amphibole; Kf = K-feldspar; Bi = biotite; Ttn = titanite; Se = sericite.

Middle Jurassic (164 Ma) Tongshanling granites, the Late Jurassic (156 Ma) Jinjiling and Xishan granites (Fu et al., 2004; Jiang et al., 2009; Huang et al., 2011) and the Shuikoushan and Baoshan granodiorites in this study. Single-grain zircon U–Pb dating using a VG354 mass spectrometer suggests that the Shuikoushan and Baoshan Pb-Zn mineralized granodiorites were formed during the Middle Jurassic (173–172 Ma) (Wang et al., 2003a). However, secondary ion mass spectrometry (SIMS) and laser ablation ion coupled plasma mass spectrometry (LA–ICP–MS) zircon U–Pb dating indicate that they were generated at 162–156 Ma (Xie et al., 2013; Zuo et al., 2014a; Huang et al., 2015b; Yang et al., 2016; Zhao et al., 2017). In general, the amphibole-bearing granites in South China are suggested to have been derived either from igneous protoliths (Wang et al., 2003a; Huang et al., 2017b) or from hybridized sources that consisted of metaigneous and metasedimentary rocks (Fu et al., 2004; Jiang et al., 2009; Huang et al., 2013). In particular, the Shuikoushan and Baoshan amphibolite-bearing granites are considered to have been derived by partial melting of mantle-derived basaltic rocks with minor old crustal contamination based on whole rock element and Sr-Nd isotope characterisitcs (Wang et al., 2003a). Whole rock compositions provide only cumulative evidence for the complex process that ultimately determine magma compositions. More recently, combining whole rock element, Sr-Nd and zircon Hf-O isotope data, Yang et al. (2016) suggests that the Shuikoushan granodiorites belong to peraluminous I-type granites that were derived from middle-lower crustal amphibolites, and several other studies suggest that the Shuikoushan and Baoshan granodiorites were possibly generated by the anatexis of old crustal components triggered by the input of mantle-derived magma since they have higher $Mg^{\#}$ values than experimental melts from pure crustal basaltic rocks (Xie et al., 2013; Zuo et al., 2014b; Zhao et al., 2017). Because the Shuikoushan and Baoshan granodiorites are associated with Pb-Zn mineralization (Huang et al., 2015b; Xie et al., 2015), in this study, we suggest that major elements such as Al_2O_3, CaO, Na_2O, K_2O, $Fe_2O_3^T$ and MgO were possibly mobile during hydrothermal alteration. Therefore, the A/CNK and $Mg^{\#}$ values may not be primitive features. Whether a metasedimentary rock played an important role in the formation of amphibole-bearing granites remains unclear.

Recent research suggests that zircon oxygen isotope is an effective tracer of sedimentary rocks in the source of granitic magmas (Kemp et al., 2007; Li et al., 2009, 2010a; Huang et al., 2011; Jiao et al., 2015; Rong et al., 2017). Zircons from sedimentary rock-derived granites commonly show high $\delta^{18}O$ values (> 8.1‰; Wu et al., 2006b; Zheng et al., 2007). In this study, we report new zircon LA–ICP–MS U–Pb ages, whole-rock elemental and Sr–Nd isotopic analyses, and zircon Hf–O isotopic analyses of the Shuikoushan and Baoshan granodiorites in the western Nanling Range in order to identify the contribution of

Table 1
LA-ICP-MS zircon U-Pb isotopic data of the Shuikoushan and Baoshan granodiorites in the western Nanling Range.

	Contents (ppm)				Isotopic ratios						Isotopic ages (Ma)					
Points	Th	U	Pb	Th/U	$^{207}Pb/^{206}Pb$	1σ	$^{207}Pb/^{235}U$	1σ	$^{206}Pb/^{238}U$	1σ	$^{207}Pb/^{206}Pb$	1σ	$^{207}Pb/^{235}U$	1σ	$^{206}Pb/^{238}U$	1σ
								09SKS-1 Granodiorite								
1	598	734	141	0.82	0.05059	0.00091	0.17939	0.00294	0.02571	0.00046	222	18	168	3	164	3
2	184	363	47.4	0.51	0.05338	0.00193	0.18619	0.00612	0.02530	0.00057	345	37	173	5	161	4
3	94.0	294	26.2	0.32	0.05230	0.00183	0.18503	0.00591	0.02566	0.00056	299	36	172	5	163	4
4	247	437	64.0	0.57	0.05087	0.00109	0.18023	0.00355	0.02569	0.00047	235	20	168	3	164	3
5	165	565	46.0	0.29	0.04993	0.00179	0.17650	0.00579	0.02563	0.00057	192	38	165	5	163	4
6	127	297	33.8	0.43	0.05180	0.00251	0.17747	0.00789	0.02485	0.00064	277	56	166	7	158	4
7	214	405	52.5	0.53	0.04894	0.00100	0.17126	0.00322	0.02538	0.00046	145	20	161	3	162	3
8	275	400	68.0	0.69	0.05258	0.00107	0.18671	0.00347	0.02575	0.00047	311	19	174	3	164	3
9	238	399	60.0	0.60	0.05231	0.00102	0.19031	0.00338	0.02639	0.00047	299	19	177	3	168	3
10	354	472	89.0	0.75	0.05435	0.00651	0.19457	0.02131	0.02596	0.00138	386	152	181	18	165	9
11	157	411	42.3	0.38	0.05271	0.00289	0.18643	0.00942	0.02565	0.00070	316	66	174	8	163	4
12	174	388	41.7	0.45	0.04975	0.00103	0.17080	0.00325	0.02490	0.00045	183	20	160	3	159	3
13	188	392	46.8	0.48	0.04898	0.00103	0.16773	0.00323	0.02483	0.00045	147	20	157	3	158	3
14	148	254	35.7	0.58	0.04606	0.00400	0.15477	0.01305	0.02437	0.00050	191	1	146	11	155	3
15	152	300	42.3	0.51	0.04629	0.00279	0.16009	0.00915	0.02509	0.00048	132	12	151	8	160	3
16	115	313	29.4	0.37	0.04911	0.00228	0.16994	0.00727	0.02510	0.00062	153	56	159	6	160	4
17	244	434	56.0	0.56	0.04688	0.00099	0.16528	0.00320	0.02557	0.00046	43	21	155	3	163	3
18	164	294	39.3	0.56	0.04971	0.00124	0.17137	0.00396	0.02501	0.00047	181	24	161	3	159	3
19	233	404	55.5	0.58	0.05282	0.00115	0.18137	0.00361	0.02490	0.00045	321	20	169	3	159	3
20	422	570	96.0	0.74	0.04992	0.00086	0.17483	0.00272	0.02540	0.00044	191	18	164	2	162	3
								09BS05 Granodiorite								
1	143	379	33.0	0.38	0.04927	0.00082	0.17262	0.00260	0.02535	0.00043	161	18	162	2	161	3
2	217	601	56.1	0.36	0.04726	0.00065	0.16559	0.00202	0.02536	0.00042	62	19	156	2	161	3
3	855	781	196	1.09	0.05374	0.00074	0.18858	0.00230	0.02541	0.00042	360	18	175	2	162	3
4	311	701	83.2	0.44	0.05140	0.00060	0.17965	0.00183	0.02531	0.00041	259	20	168	2	161	3
5	179	417	42.5	0.43	0.04974	0.00114	0.17277	0.00359	0.02516	0.00046	183	22	162	3	160	3
6	339	792	88.6	0.43	0.05134	0.00096	0.17952	0.00302	0.02533	0.00045	256	18	168	3	161	3
7	418	872	98.9	0.48	0.04801	0.00062	0.16790	0.00192	0.02534	0.00042	100	19	158	2	161	3
8	299	753	73.9	0.40	0.04794	0.00075	0.16768	0.00235	0.02536	0.00043	96	18	157	2	161	3
9	215	615	46.3	0.35	0.04739	0.00057	0.16688	0.00178	0.02554	0.00042	69	20	157	2	163	3
10	143	413	35.2	0.35	0.04956	0.00076	0.17196	0.00238	0.02517	0.00043	174	18	161	2	160	3
11	318	477	66.1	0.67	0.04815	0.00065	0.16799	0.00203	0.02531	0.00043	107	20	158	2	161	3
12	171	416	43.8	0.41	0.04820	0.00073	0.16853	0.00230	0.02536	0.00043	109	18	158	2	161	3
13	238	692	54.4	0.34	0.04940	0.00059	0.17298	0.00182	0.02540	0.00043	167	21	162	2	162	3
14	160	428	39.2	0.37	0.05091	0.00072	0.17811	0.00225	0.02538	0.00043	237	18	166	2	162	3
15	381	369	85.9	1.03	0.04939	0.00165	0.16943	0.00519	0.02489	0.00053	166	35	159	5	158	3
16	244	508	57.8	0.48	0.05471	0.00069	0.19107	0.00217	0.02534	0.00043	400	19	178	2	161	3
17	262	514	69.3	0.51	0.04876	0.00073	0.17078	0.00231	0.02542	0.00044	136	19	160	2	162	3
18	371	552	84.9	0.67	0.04841	0.00070	0.16923	0.00221	0.02537	0.00044	119	19	159	2	162	3
19	397	891	95.1	0.45	0.04606	0.00291	0.15986	0.00965	0.02517	0.00046	138	1	151	8	160	3
20	725	1249	195	0.58	0.05191	0.00062	0.18069	0.00192	0.02526	0.00043	281	21	169	2	161	3

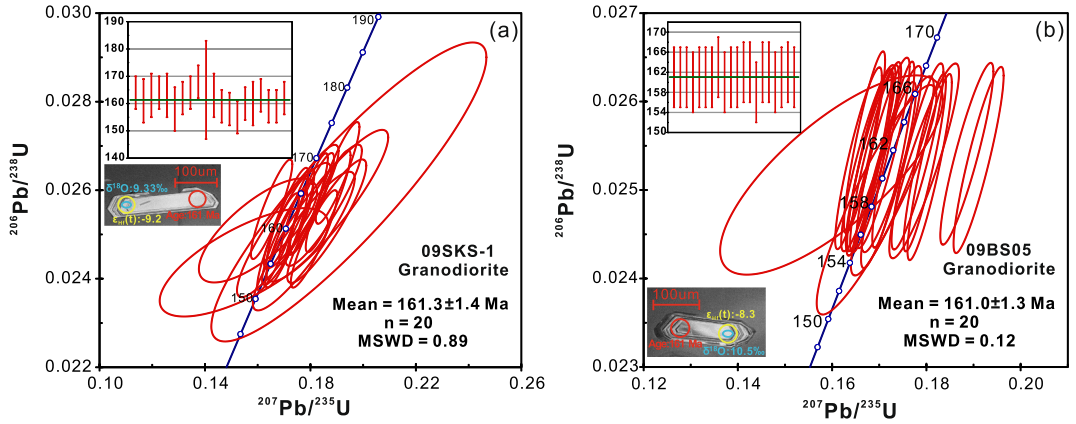

Fig. 3. LA–ICP–MS zircon U–Pb concordia diagrams for: (a) sample 09SKS-1 (granodiorite) and (b) sample 09BS05 (granodiorite).

sedimentary rocks and provide new insights into the genesis of amphibole-bearing granites.

2. Geological setting and petrography

The SCB which consists of its northwest Yangtze Block and its southeast Cathaysia Block (Wang et al., 2003b; Zhou et al., 2006) is bounded by the Pacific Ocean to the east, the Longmenshan Fault Zone and Ailaoshan–Honghe Fault to the west, the Qinling–Dabie–Sulu ultrahigh-pressure tectonic belt to the north, and the South China Sea to the south (Fig. 1a). The Yangtze and Cathaysia blocks are commonly believed to have amalgamated along the Jiangnan Orogenic Belt during

Table 2
Major (wt%) and trace (ppm) elements data for the Shuikoushan and Baoshan granodiorites in the western Nanling Range.

Sample	09BS02	09BS03	09BS04	09BS05	09SKS-1	09SKS-2	09SKS-3
SiO_2	69.95	69.82	61.76	70.72	63.25	63.53	62.00
TiO_2	0.28	0.27	0.53	0.24	0.75	0.65	0.73
Al_2O_3	13.50	13.34	16.59	13.33	15.63	16.05	14.80
$Fe_2O_3^T$	2.67	2.60	6.25	2.08	3.98	5.03	5.61
MnO	0.07	0.07	0.34	0.06	0.06	0.28	0.06
MgO	1.14	1.12	1.77	1.23	2.22	1.01	2.00
CaO	1.68	1.55	6.03	1.18	3.75	3.45	4.55
Na_2O	1.42	1.91	0.83	1.93	0.15	0.20	0.37
K_2O	4.93	5.01	1.74	5.06	3.71	3.47	2.75
P_2O_5	0.09	0.09	0.23	0.08	0.36	0.31	0.36
L.O.I	3.92	3.74	3.53	3.75	5.96	5.84	6.69
Total	99.65	99.52	99.6	99.66	99.82	99.82	99.92
$Mg^{\#}$	0.46	0.46	0.36	0.54	0.52	0.28	0.41
Sc	4.60	5.56	3.58	4.43	16.2	15.0	17.6
V	44.2	44.5	30.1	39.6	164	149	169
Cr	1.90	3.95	0.480	2.44	37.7	31.8	52.0
Co	17.2	24.1	13.7	16.7	38.6	27.2	19.8
Ni	2.05	2.07	1.89	1.79	10.2	11.4	14.7
Cu	2.62	2.73	1.98	2.61	70.8	160	160
Zn	37.7	35.5	27.1	28.0	39.5	153	58.7
Ga	15.2	16.0	13.8	14.7	18.6	21.0	18.1
Ge	1.84	2.13	1.62	1.81	3.01	4.91	2.08
Rb	126	149	172	146	175	188	133
Sr	147	181	164	152	110	135	57.7
Y	15.4	16.3	14.8	13.4	17.8	20.7	19.8
Zr	106	119	133	108	189	169	170
Nb	15.9	16.6	14.6	16.0	16.5	15.6	15.4
Cs	22.0	21.5	23.2	24.7	44.2	30.2	34.4
Ba	389	474	350	375	723	236	349
La	21.2	21.6	18.5	24.6	32.0	54.4	37.6
Ce	41.2	43.3	36.3	46.4	61.9	105	75.7
Pr	4.88	4.95	4.40	5.44	7.38	12.4	9.04
Nd	17.4	17.6	15.7	19.2	27.5	46.6	33.1
Sm	3.26	3.31	3.04	3.46	5.04	7.71	5.93
Eu	0.890	0.960	0.860	0.860	1.19	1.67	1.32
Gd	2.87	2.90	2.70	2.84	4.46	6.24	5.06
Tb	0.460	0.470	0.440	0.450	0.630	0.790	0.710
Dy	2.79	2.79	2.68	2.54	3.4	4.06	3.79
Ho	0.580	0.600	0.580	0.530	0.640	0.780	0.720
Er	1.82	1.84	1.79	1.67	1.86	2.24	2.06
Tm	0.300	0.310	0.300	0.290	0.270	0.330	0.310
Yb	2.22	2.23	2.22	2.13	1.76	2.14	2.15
Lu	0.350	0.370	0.360	0.340	0.270	0.320	0.340
Hf	3.06	3.40	3.73	3.20	4.13	3.66	3.77
Ta	1.73	1.86	1.71	1.80	1.19	1.06	1.09
Pb	29.7	30.3	32.5	30.0	6.62	62.6	14.7
Th	14.9	16.8	15.3	16.6	13.8	13.5	13.2
U	4.10	4.69	4.32	4.17	2.67	3.71	3.43
Th/La	0.70	0.78	0.82	0.68	0.43	0.25	0.35
ΣREE	100	103	90	111	148	245	178

Note: Mg# = molar MgO/(molar MgO + molar FeO), assuming FeO = 0.8998 × $Fe_2O_3^T$.

the Neoproterozoic (Zhao, 2015). After the amalgamation of Yangtze and Cathaysia, the SCB experienced the Caledonian and Indosinian orogenies at 460–415 Ma and 250–205 Ma, respectively (Wang et al., 2007, 2011b). One of the geological signatures associated with the Caledonian and Indosinian orogenies is widespread granitic rocks (Bai et al., 2007; Wang et al., 2007, 2011b; Yu et al., 2007; Gao et al., 2014). However, most of the granitic rocks in the SCB were formed during the Late Mesozoic (Fig. 1b; Zhou et al., 2006; Li et al., 2007), and they form a ~ 600 km wide volcanic–intrusive belt, parallel to the present coastline (Jiang et al., 2009). Some of these granitoids are associated with Cu–Pb–Zn (or W–Sn) mineralization (He et al., 2010; Huang et al., 2015b).

Middle to Late Jurassic felsic and mafic magmatic rocks are widespread in the western Nanling Range (Fig. 1b; Jiang et al., 2008, 2009; Zhao et al., 2012). The granitic intrusions include the Baoshan, Shuikoushan, Tongshanling, Tongan, Niumiao, Qianlishan, Qitianling, Jinjiling, Xishan, Huashan, and Guposhan intrusions (Wang et al., 2003a; Zhu et al., 2005; Jiang et al., 2008; Zhao et al., 2012). Mafic rocks occur sporadically, including the Ningyuan, Changchengling, and Daoxian basaltic lavas, and the Guiyang lamprophyre dykes (Fig. 1b; Wang et al., 2003b, 2008b; Li et al., 2004; Jiang et al., 2009).

The Shi–Hang zone (Fig. 1a, b) is a NE-trending belt of granites that are characterized by high Sm (> 8 ppm) and Nd (> 45 ppm) contents, as well as relatively high $\varepsilon_{Nd}(t)$ values (> −8.0), young T_{DM} model ages (< 1.5 Ga), and relatively low initial $^{87}Sr/^{86}Sr$ ratios (< 0.710; Gilder et al., 1996; Chen and Jahn, 1998; Zhou et al., 2006; Jiang et al., 2008). The Shuikoushan and Baoshan granitic plutons, along with the Qianlishan, Qitianling, Jinjiling, Xishan, Huashan and Guposhan granitic plutons, constitute a NE-trending magmatic zone south of the Shi–Hang zone (Fig. 1b; Gilder et al., 1996; Zhao et al., 2012). Economically significant Pb–Zn and W–Sn mineralizations in the region are genetically associated with these granitoids (Huang et al., 2015b). The Shuikoushan granodiorites are associated with Pb–Zn–Au mineralization, while the Baoshan granodiorites are linked with Pb–Zn–Cu–Mo mineralization (Lu et al., 2006; Huang et al., 2015b). The Shuikoushan and Baoshan granodiorites are small in volume, occur as veins, laccoliths, lopoliths, and knobs, and crop out over an area that is 1.2–1.6 km wide and 1.6–4.6 km long (Wang et al., 2003a; Yang et al., 2016). They intruded Carboniferous limestone and Permian sandstone and shale (Fig. 1c). The Shuikoushan plutons are dominantly biotite-amphibole granodiorites, composed of 30–50 vol% plagioclase, 10–20 vol% K-feldspar, 20–30 vol% quartz, 3–5 vol% amphibole, and 10–15 vol% biotite. Accessory minerals include zircon, apatite, pyrite, magnetite, allanite and titanite. Quartz and titanite commonly coexist with biotite (Fig. 2a, b). Most of plagioclases have been replaced by sericites (Fig. 2a, b). The Baoshan plutons are dominantly biotite-amphibole granodiorite porphyries. Their phenocrysts are K-feldspar (15–20 vol %), plagioclase (5 vol%), quartz (5 vol%), amphibole (3–5 vol%), and biotite (5–8 vol%) (Fig. 2c, d). The matrix has a microgranular or fine granular texture, and consists of hypidiomorphic plagioclase, K-feldspar, amphibole, biotite, and xenomorphic quartz. Accessory minerals include apatite, zircon, allanite, titanite, and magnetite. Small titanite and biotite crystals commonly coexist with K-feldspar (Fig. 2e). The coexsolution of quartz and K-feldspar led to a vermicular texture (Fig. 2f).

3. Analytical methods

3.1. Zircon U–Pb dating

Cathodoluminescence (CL) images of zircon crystals were obtained prior to analysis using a Mono CL3 + detector (Gatan, Pleasanton, CA, USA) attached to a field emission electron microscope (Supra 55 Sapphire, Zeiss, Germany) at the State Key Laboratory of Isotope Geochemistry (SKLaBIG), Guangzhou Institute of Geochemistry, Chinese Academy of Sciences (GIG–CAS), Guangzhou, China.

Zircon U–Pb dating on two samples was performed by LA–ICP–MS at the Institute of Geology and Geophysics, Chinese Academy of Sciences (IGG–CAS), Beijing, China. Detailed operating conditions for the LA–ICP–MS and data reduction were described by Xie et al. (2008). A Neptune multi-collector (MC)–ICP–MS was connected to a 193-nm excimer ArF laser ablation cell via a mixing chamber. Every spot analysis consisted of ~30 s of background acquisition and 40 s of data acquisition. Zircon 91,500 and silicate glass NIST 610 were used as standards, and the beam diameter was 44 μm. Element corrections were determined relative to NIST 610. The age calculations were made using ICPMSDataCal (Version 8.4; Liu et al., 2008) and plots were made using Isoplot 3.75 (Ludwig, 2012).

3.2. Major and trace element analyses

Major-element oxides were measured in fused glass beads using a Rigaku RIX 2000 X-ray fluorescence spectrometer with analytical

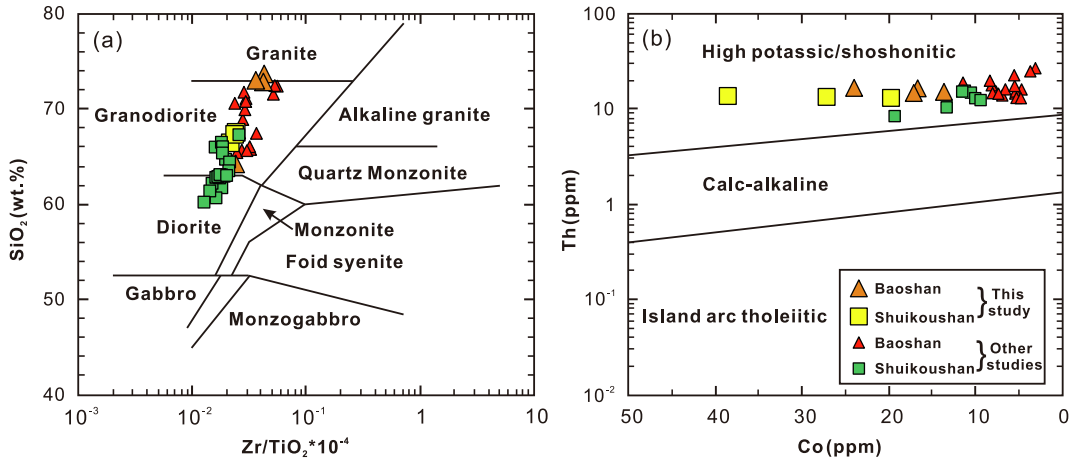

Fig. 4. (a) $Zr/TiO_2 \times 10^{-4}$ vs. SiO_2 rock classification diagram (modified from Winchester and Floyd, 1977). (b) Co vs. Th diagram (modified from Hastie et al., 2007). Data for the Shuikoushan and Baoshan granodiorites are from this study, Wang et al. (2003a), Xie et al. (2013), and Yang et al. (2016).

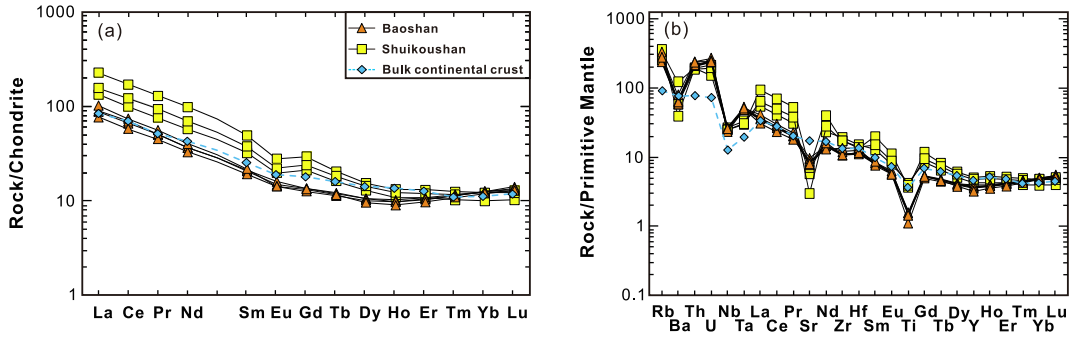

Fig. 5. (a) Chondrite-normalized REE plots of the Shuikoushan and Baoshan granodiorites. (b) Primitive mantle-normalized spider diagrams for the Shuikoushan and Baoshan granodiorites. Normalizing values and bulk continental crust reference curves are from Sun and McDonough (1989) and Rudnick and Gao (2003), respectively.

uncertainties < 5% at SKLaBIG, GIG–CAS. Details of the analytical procedures are provided by Li et al. (2002). Trace elements and REE were analyzed using a Perkin–Elmer SCIEX ELAN 6000 ICP–MS at the SKLaBIG, GIG–CAS. About 40 mg of each powered sample was dissolved in a high-pressure Teflon bomb for 48 h at ~190 °C using a HF + HNO_3 + $HClO_4$ mixture. An internal standard solution containing Rh and Re was used to monitor signal drift during counting. The international standards BHVO-2, GSR-1, GSR-2, GSR-3, SARM-4, AGV-2, and W-2a were used for analytical quality control, and analytical precision was better than 2%–5% RSD (relative standard deviation) for most trace elements. The details of analytical procedures are described by Li et al. (2002).

3.3. Whole-rock Sr–Nd isotope analyses

Sr and Nd isotope analyses of selected samples were carried out at the SKLaBIG, GIG–CAS using a Micromass IsoProbe MC–ICP–MS. The sample powders were mixed with nitric and hydrofluoric acids, digested in Teflon containers, then processed through Sr (AGW50-X12) and Nd (HDEHP) cation exchange columns for element separation. The measured $^{87}Sr/^{86}Sr$ ratio of the NBS987 standard and $^{143}Nd/^{144}Nd$ ratio of the Shin Etsu JNdi-1 standard were 0.710285 ± 0.000015 (2σ) and 0.512090 ± 0.000009 (2σ), respectively. All measured $^{143}Nd/^{144}Nd$ and $^{86}Sr/^{88}Sr$ ratios were corrected for fractionation to $^{146}Nd/^{144}Nd$ = 0.7219 and $^{86}Sr/^{88}Sr$ = 0.1194, respectively. The details of the analytical procedures are described by Wei et al. (2002) and Liang et al. (2003).

3.4. Zircon oxygen isotope analysis

Zircon oxygen isotope was measured using a CAMECA IMS 1280 SIMS at the IGG–CAS. Analytical procedures are described by Li et al. (2010a), with data reported as per mil (‰) relative to Vienna Standard Mean Ocean Water (VSMOW, $^{18}O/^{16}O$ = 0.0020052). Uncertainties on individual analyses are reported at the 2σ level, with an internal precision better than 0.2‰. The instrumental mass fractionation factor (IMF) was corrected using the Penglai zircon standard ($\delta^{18}O$ = 5.31 ± 0.10‰; Li et al., 2010b). The Qinghu zircon standard was analyzed as an unknown, alternating with our sample zircon, to monitor the external uncertainties. The weighted mean measured $\delta^{18}O$ value of the Qinghu zircon standard is within error of the reported value of 5.39 ± 0.22‰ (2σ; Li et al., 2013a,b).

3.5. In situ zircon Hf isotope analysis

In situ zircon Hf isotope analysis was made by MC–ICP–MS at the IGG–CAS, with a beam size of 45 μm and laser pulse frequency of 8 Hz. Details of the instrumental conditions and data acquisition are given by Wu et al. (2006a). The isobaric interference of ^{176}Lu on ^{176}Hf is negligible, due to the extremely low $^{176}Lu/^{177}Hf$ in zircon (normally < 0.002). During this study, the GJ-1 reference zircon was analyzed as an unknown sample, yielding a weighted mean $^{176}Hf/^{177}Hf$ ratio of 0.282018 ± 0.000020 ($2\sigma_n$, n = 10), which is in good agreement with the recommended value of 0.282000 ± 0.000005 (Morel et al., 2008). During the acquisition of the Hf isotope data, the weighted mean measured $^{176}Hf/^{177}Hf$ ratio of the zircon standard Mud Tank was 0.282504 ± 0.000003 ($2\sigma_n$, n = 10), which is also in good agreement

Table 3
Sr and Nd isotope data for the Shuikoushan and Baoshan granodiorites in the western Nanling Range.

Sample	Contents (ppm)											Age (Ma)		Reference
	Sm	Nd	Rb	Sr	$(^{87}Sr/^{86}Sr)_s$	$(^{87}Rb/^{86}Sr)_s$	$(^{147}Sm/^{144}Nd)_s$	$(^{143}Nd/^{144}Nd)_s$	$(^{87}Sr/^{86}Sr)_i$	$(^{143}Nd/^{144}Nd)_i$	$\varepsilon_{Nd}(t)$	T_{DM}	T_{2DM}	
09BS04	3.04	15.7	172	164	0.721416	3.046	0.118	0.512172	0.714498	0.512048	−7.5	1549	1566	This study
09BS05	3.46	19.2	146	152	0.722748	2.781	0.110	0.512188	0.716432	0.512071	−7.0	1408	1529	This study
BSH-2	5.11	24.8	183	79.8	0.725834	6.634	0.125	0.512213	0.710651	0.512081	−6.8	1618	1515	Wang et al. (2003a)
BSH-4	5.19	25.8	189	65.1	0.730297	8.398	0.122	0.512253	0.711075	0.512124	−6.0	1499	1446	Wang et al. (2003a)
BSH-6	5.46	28.6	186	74.8	0.727253	7.193	0.116	0.512227	0.710789	0.512105	−6.4	1444	1477	Wang et al. (2003a)
BSH-7	4.83	24.3	173	79.7	0.725769	6.279	0.121	0.512263	0.711397	0.512136	−5.8	1459	1428	Wang et al. (2003a)
16903–70	5.55	31.6	147	310	0.712592	1.372	0.107	0.512286	0.709452	0.512173	−5.0	1235	1367	Xie et al. (2013)
15801–03	6.29	44.4	281	98.8	0.727839	8.227	0.086	0.512264	0.709008	0.512173	−5.0	1061	1368	Xie et al. (2013)
11BS-46	4.08	22.3	133	78.5	0.721666	4.901	0.111	0.512177	0.710448	0.512060	−7.2	1450	1549	Xie et al. (2013)
11BS-69	5.70	39.4	305	130	0.725249	6.787	0.088	0.512269	0.709715	0.512176	−5.0	1070	1363	Xie et al. (2013)
11BS-72	4.41	24.6	194	142	0.719605	3.952	0.109	0.512179	0.710559	0.512064	−7.2	1416	1542	Xie et al. (2013)
09SKS-1	5.04	27.5	175	110	0.721484	4.631	0.112	0.512278	0.710965	0.512160	−5.3	1299	1387	This study
09SKS-2	7.71	46.6	188	135	0.721927	4.046	0.101	0.512273	0.712739	0.512167	−5.1	1181	1377	This study
SKS-1	4.36	20.9	136	78.6	0.721045	5.005	0.127	0.512253	0.709589	0.512119	−6.1	1577	1454	Wang et al. (2003a)
SKS-3	5.07	28.5	189	100	0.723729	5.489	0.108	0.512219	0.711165	0.512105	−6.4	1347	1476	Wang et al. (2003a)
SKS-7	8.61	38.2	84.0	309	0.711467	0.786	0.137	0.512272	0.709667	0.512127	−5.9	1749	1440	Wang et al. (2003a)
SKS-9	8.66	37.8	77.6	306	0.711527	0.734	0.139	0.512280	0.709848	0.512133	−5.8	1785	1432	Wang et al. (2003a)
SKS-6	6.38	34.0	132	491	0.711854	0.778	0.114	0.512231	0.710074	0.512111	−6.2	1409	1467	Yang et al. (2016)
SKS-31	6.44	32.5	135	510	0.71182	0.766	0.121	0.512255	0.710067	0.512128	−5.9	1466	1440	Yang et al. (2016)
SKS-36	6.13	31.9	114	441	0.711845	0.748	0.117	0.512241	0.710133	0.512118	−6.1	1433	1456	Yang et al. (2016)
SKS-50	6.49	34.6	133	491	0.711864	0.784	0.114	0.512248	0.710071	0.512128	−5.9	1382	1440	Yang et al. (2016)

$^{87}Rb/^{86}Sr$ and $^{147}Sm/^{144}Nd$ are calculated using whole-rock Rb, Sr, Sm and Nd contents in Table 2;
$(^{87}Sr/^{86}Sr)_i = (^{87}Sr/^{86}Sr)_S-(^{87}Rb/^{86}Sr)_S \times (e^{\lambda t}-1)$, $(^{87}Sr/^{86}Sr)_S$ and $(^{87}Rb/^{86}Sr)_S$ are values of analysed sample; $\lambda = 1.42 \times 10^{-11}$ year^{-1};
$\varepsilon_{Nd}(t) = 10{,}000 \times \{[(^{143}Nd/^{144}Nd)_s-(^{147}Sm/^{144}Nd)_s \times (e^{\lambda t}-1)]/[(^{143}Nd/^{144}Nd)_{CHUR(0)}-(^{147}Sm/^{144}Nd)_{CHUR} \times (e^{\lambda t}-1)]-1\}$;
$T_{DM} = \ln[(^{143}Nd/^{144}Nd)_s-(^{143}Nd/^{144}Nd)_{DM}] / [(^{147}Sm/^{144}Nd)_s-(^{147}Sm/^{144}Nd)_{DM}]/\lambda_{Sm}$;
$T_{2DM} = T_{DM}-(T_{DM}-t) \times [(f_{cc}-f_{Sm/Nd})/(f_{cc}-f_{DM})]$, $f_{Sm/Nd} = (^{147}Sm/^{144}Nd)_s/(^{147}Sm/^{144}Nd)_{CHUR}-1$ (Depaolo, 1981).
In the calculation, $(^{143}Nd/^{144}Nd)_{CHUR} = 0.512638$, $(^{147}Sm/^{144}Nd)_{CHUR} = 0.1967$, $(^{143}Nd/^{144}Nd)_{DM} = 0.513151$, $(^{147}Sm/^{144}Nd)_{DM} = 0.2135$, $(^{147}Sm/^{144}Nd)_{CC} = 0.12$, $\lambda_{Sm} = 6.54 \times 10^{-12}$ year^{-1} and t = 161 Ma.

with the recommended value of 0.282511 ± 0.000036 (Hu et al., 2012).

4. Results

4.1. Zircon U–Pb geochronology

Zircon U–Pb isotopic data are given in Table 1. One Shuikoushan sample (09SKS-1) and one Baoshan sample (09BS05) were selected for LA–ICP–MS zircon U–Pb dating. Zircon crystals in 09SKS-1 have lengths of 100 to 300 μm, with length/width ratios of 2:1–3:1 (Fig. 3a), whereas zircon crystals in 09BS05 have lengths of 100–150 μm, with the same length/width ratios (Fig. 3b). Well-developed oscillatory zoning and high Th/U ratios (Table 1) indicate a magmatic origin for these zircon crystals (Hoskin and Black, 2000). Twenty analyses of zircons in 09SKS-1 gave $^{206}Pb/^{238}U$ ages of 155 to 168 Ma, with a weighted mean age of 161.3 ± 1.4 Ma (MSWD = 0.89, n = 20; Fig. 3a). Twenty analyses of zircons in 09BS05 gave $^{206}Pb/^{238}U$ ages of 158–163 Ma, with a weighted mean age of 161.0 ± 1.3 Ma (MSWD = 0.12, n = 20; Fig. 3b). Adding our data to other SIMS and LA–ICP–MS zircon U–Pb ages for the Shuikoushan and Baoshan intrusive rocks (156–162 Ma; Lu et al., 2006; Xie et al., 2013; Zuo et al., 2014a; Huang et al., 2015b; Yang et al., 2016; Zhao et al., 2017), we suggest that the Shuikoushan and Baoshan granodiorites were emplaced during the Late Jurassic (ca. 161 Ma).

4.2. Major and trace element geochemistry

The Shuikoushan and Baoshan granodiorites exhibit relatively large variations of SiO_2 (61.8–70.7 wt%), $Fe_2O_3^T$ (2.08–6.25 wt%), MgO (1.01–2.22 wt%) and TiO_2 (0.24–0.75 wt%) contents (Table 2), and relatively high Al_2O_3 (13.3–16.6 wt%) contents (Table 2). They plot mainly in the granodiorite field on the Zr/TiO_2 vs. SiO_2 diagram (Fig. 4a) and the high-K or shoshonitic fields on the Co vs. Th diagram (Fig. 4b), with varied $Mg^{\#}$ (0.28–0.54; Table 2).

The Shuikoushan and Baoshan granodiorites have slightly enriched rare earth element (REE) concentrations (ΣREE = 90 to 245 ppm; Table 2) relative to bulk continental crust (Rudnick and Gao, 2003). REE concentrations of the Shuikoushan granodiorites are higher than that of the Baoshan granodiorites (Fig. 5a; Table 2). They reveal steep LREE with $[La/Sm]_N$ (where 'N' indicates normalized to chondrite) ratios between 3.93 and 4.59 and relatively flat HREE patterns with $[Gd/Yb]_N$ ratios range from 1.01 to 2.41 (Fig. 5a) on chondrite-normalized REE diagram. In addition, they have weakly negative to negligible Eu anomalies ($\delta Eu = [Eu_N/(Sm_N \times Gd_N)^{1/2}] = 0.74$ to 0.95; Fig. 5a). The Shuikoushan and Baoshan granodiorites also show negative Nb, Ta and Ti and positive Th and U anomalies on primitive mantle-normalized trace element diagram (Fig. 5b).

4.3. Whole-rock Sr–Nd and in situ zircon Hf–O isotope compositions

In this study, initial Sr-Nd isotopic ratios have been calculated at 161 Ma, on the basis of the LA-ICP-MS zircon U-Pb ages for the Shuikoushan and Baoshan granodiorites. The Shuikoushan and Baoshan granodiorites have evolved radiogenic isotope compositions, with present day $^{87}Sr/^{86}Sr$ ratios of 0.721416–0.722748 and $^{143}Nd/^{144}Nd$ ratios of 0.512172–0.512278, corresponding to $(^{87}Sr/^{86}Sr)_i$ ratios of 0.7110–0.7164 and $\varepsilon_{Nd}(t)$ values of −7.5 to −5.1 (Table 3; Fig. 6a). Their two-stage Nd model ages (T_{2DM}) range from 1.38 to 1.57 Ga (Table 3).

Samples 09SKS-1 and 09BS05 were also selected for zircon Hf and O isotopic analyses (Table 4). Sample 09SKS-1 exhibits relatively small variations of zircon Hf as well as O isotopic compositions. Their measured $^{176}Hf/^{177}Hf$ ratios and $\varepsilon_{Hf}(t)$ values vary from 0.282280 to 0.282435 and −13.9 to −8.5, respectively (Table 4; Figs. 6b–c and 7a). They also show high $\delta^{18}O$ values of 8.8‰–11.9‰ (Table 4). They only display a major peak on $\varepsilon_{Hf}(t)$ and $\delta^{18}O$ frequency distribution histograms (Fig. 7a, b). Average $\varepsilon_{Hf}(t)$ and $\delta^{18}O$ values of 09SKS-1 are

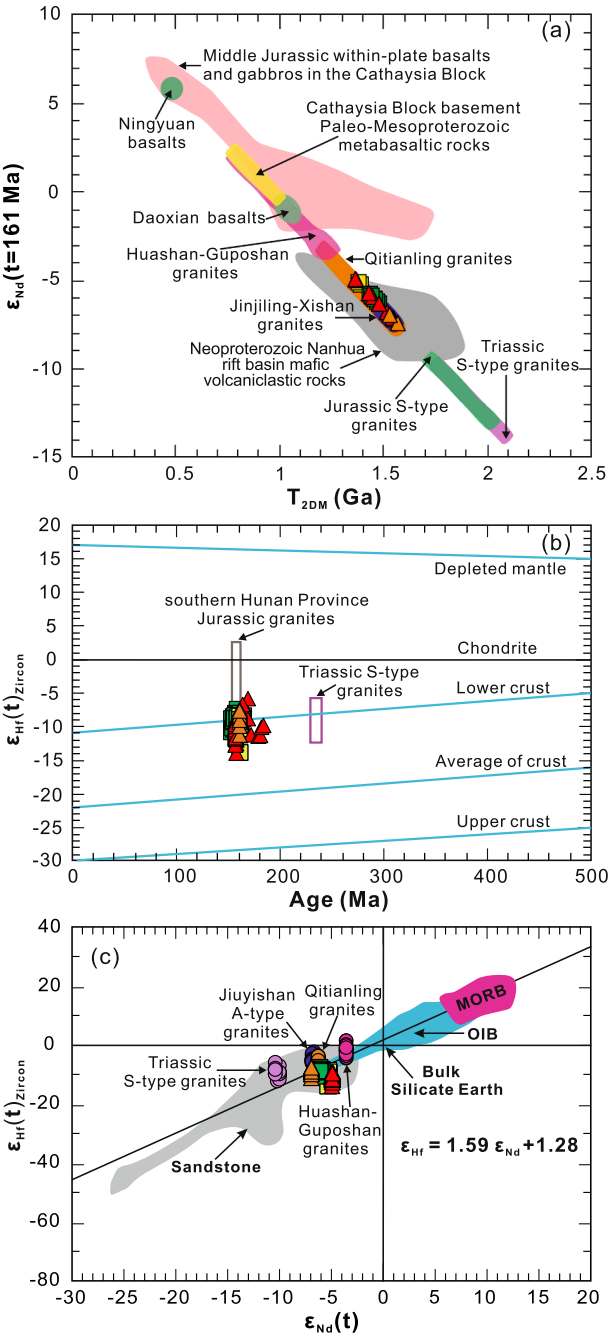

Fig. 6. (a) Two-stage Nd model ages (T_{2DM}) vs. ε_{Nd} (t = 161 Ma) for the Shuikoushan and Baoshan granodiorites and the Huashan–Guposhan granites (Zhu et al., 2006), Qitianling granites (Zhao et al., 2012), Jinjiling–Xishan granites (Huang et al., 2011), Middle Jurassic within-plate basalts (including the Ningyuan and Daoxian basalts) and gabbros (Li et al., 2003, 2004; Wang et al., 2003b), Jurassic S-type granites (Shen et al., 1999), Triassic S-type granites, Neoproterozoic Nanhua rift basin mafic volcaniclastic rocks and Paleo-Mesoproterozoic metabasaltic rocks in the Cathaysia Block (Yuan and Wu, 1991; Bai et al., 2007; Wang et al., 2007; Yu et al., 2007; Li et al., 2008a,b; Wang et al., 2008a; Wang et al., 2011a; Gao et al., 2014; Jiang and Zhu, 2017, and references therein). The initial Nd isotopic compositions of Jurassic S-type granites, Triassic S-type granites, Neoproterozoic Nanhua rift basin mafic volcaniclastic rocks and Paleo-Mesoproterozoic metabasaltic rocks are recalculated to 161 Ma. (b) Hf isotope evolution in the zircon from the Shuikoushan and Baoshan granodiorites, depleted mantle with present-day $^{176}Lu/^{177}Hf$ = 0.0384 and $^{176}Hf/^{177}Hf$ = 0.28325 (Griffin et al., 2000), chondrite with present-day $^{176}Lu/^{177}Hf$ = 0.0332 and $^{176}Hf/^{177}Hf$ = 0.28277 (Wu et al., 2007b, and references therein), continental upper crust with present-day $^{176}Lu/^{177}Hf$ = 0.0093, average crust with present-day $^{176}Lu/^{177}Hf$ = 0.015, and lower crust with present-day $^{176}Lu/^{177}Hf$ = 0.022 (Wu et al., 2007b, and references therein). Data are from Quan et al. (2012), Xie et al. (2013), Zuo et al. (2014a), and Yang et al. (2016). The western Nanling Range Jurassic granites include the Qianlishan (Chen et al., 2016), Qitianling (Zhao et al., 2012), and Huashan–Guposhan (Wang et al., 2014) granites. Triassic S-type granites in the Cathaysia Block include the Fucheng (Yu et al., 2007; Gao et al., 2014), Luxi, and Xiazhuang intrusions (Gao et al., 2014). (c) Zircon $\varepsilon_{Hf}(t)$ vs. whole rock $\varepsilon_{Nd}(t)$ diagram (modified from Chauvel et al., 2008). Endmember data (MORB, OIB, and sandstone) are from Richards et al. (2005), Chauvel et al. (2008), and references therein. Data for the Huashan–Guposhan, Qitianling, Jinjiling–Xishan, and Triassic S-type granites in the Cathaysia Block are from Wang et al. (2014), Zhao et al. (2012), Huang et al. (2011), and Gao et al. (2014), respectively.

−9.8 ± 0.5 (2σ; Fig. 7a) and 9.3 ± 0.3‰ (2σ; Fig. 7b), respectively. Similar to 09SKS-1, sample 09BS05 also exhibits relatively small variations of zircon Hf−O isotopic compositions. Their measured $^{176}Hf/^{177}Hf$ ratios and $\varepsilon_{Hf}(t)$ values vary from 0.282356 to 0.282466 and −11.3 to −7.5, respectively (Table 4; Figs. 6b–c, 7c). They also show high $\delta^{18}O$ values between 9.1‰ and 10.5‰ (Table 4). Average $\varepsilon_{Hf}(t)$ and $\delta^{18}O$ values of 09BS05 are −8.6 ± 0.5 (2σ; Fig. 7c) and 9.7 ± 0.3‰ (2σ; Fig. 7d), respectively.

5. Discussion

5.1. Hydrothermal alteration

The Shuikoushan and Baoshan granodiorites have relatively wide ranges of loss on ignition (LOI) values (H_2O + CO_2 contents ranging from 1.8% to 8.4%), possibly resulting from varying levels of alteration (this study; Wang et al., 2003a; Xie et al., 2013; Yang et al., 2016). Generally, the transition elements (Cr, Co, Ni, Sc, and V), REE, high field strength elements (Zr, Hf and Ti) and Th remain stable during mineralizing hydrothermal alteration (Wang et al., 2006, and references therein). In addition, the SiO_2 and TiO_2 contents of the Shuikoushan and Baoshan granodiorites show no obvious variation with increasing LOI (Fig. 8a-b), indicating that they could represent original compositions of granodiorites. On the other hand, K_2O, Na_2O, Sr, and Ba contents decrease and Rb contents increase with increasing LOI (Fig. 8e, h–k). Moreover, Al_2O_3, CaO, $Fe_2O_3^T$ and MgO contents also exhibit minor variations with increasing LOI (Fig. 8c-d, f-g). Therefore, Al_2O_3, CaO, $Fe_2O_3^T$, MgO, K_2O, Na_2O, Sr, Ba, and Rb are inferred to have been mobile during hydrothermal alteration. We use mainly immobile elements, for example, SiO_2, TiO_2, high field strength elements (Zr, Hf, and Ti), REE, Th and transition elements (Cr, Co, Ni, Sc, and V), to discuss the petrogenesis of the granodiorites.

The Nd isotopic compositions of magmatic rocks are almost unaffected by hydrothermal alteration, whereas Sr isotopic compositions are susceptible readily to change (Wang et al., 2006, and references therein). Given that the $\varepsilon_{Nd}(t)$ values of the Shuikoushan and Baoshan granodiorites almost remain unchanged with increasing LOI (Fig. 8m), therefore, we consider the Nd isotopic compositions of the Shuikoushan and Baoshan granodiorites to stand for the primary isotopic information. However, samples in this study exhibit higher $(^{87}Sr/^{86}Sr)_i$ values than data of previous studies (Fig. 8l; Wang et al., 2003a; Xie et al., 2013; Yang et al., 2016). Therefore, the Sr isotopic compositions of our samples were modified to a greater extent by hydrothermal alteration than the samples of previous studies (Wang et al., 2003a; Xie et al., 2013; Yang et al., 2016). In contrast to whole rock Sr isotopic compositions, however, zircon is a stable accessory mineral that preserves the O and Hf isotope compositions of its host magma during crystallization (Li et al., 2009). Therefore, whole-rock Nd and zircon Hf–O isotope data are used to trace the source components of the Shuikoushan and Baoshan granodiorites.

Table 4
Zircon Hf-O isotopic data for the Shuikoushan and Baoshan granodiorites in the western Nanling Range.

Sample and spot	$^{176}Lu/^{177}Hf$	± 2σ	$^{176}Hf/^{177}Hf$	± 2σ	T (Ma)	$(^{176}Hf/^{177}Hf)_i$	$\varepsilon_{Hf}(t)$	± 2σ	$f_{Lu/Hf}$	T_{DM}(Ga)	T_{2DM} (Ga)	$\delta^{18}O$ (‰)	± 2σ
Sample 09BS05													
09BS05@01	0.001160	0.000010	0.282414	0.000010	161	0.282410	−9.3	0.5	−0.96	1.19	1.80	9.54	0.27
09BS05@02	0.001200	0.000010	0.282457	0.000020	161	0.282454	−7.7	0.5	−0.96	1.13	1.70	9.11	0.28
09BS05@03	0.001240	0.000020	0.282453	0.000010	162	0.282449	−7.9	0.5	−0.96	1.14	1.71	9.46	0.29
09BS05@04	0.000820	0.000010	0.282444	0.000010	161	0.282441	−8.2	0.5	−0.98	1.14	1.73	9.38	0.34
09BS05@05	0.001020	0.000010	0.282443	0.000010	160	0.282440	−8.2	0.5	−0.97	1.14	1.73	10.32	0.25
09BS05@06	0.001390	0.000010	0.282443	0.000010	161	0.282439	−8.3	0.5	−0.96	1.16	1.73	10.52	0.37
09BS05@07	0.001260	0.000010	0.282447	0.000020	161	0.282443	−8.1	0.6	−0.96	1.15	1.72	9.78	0.32
09BS05@08	0.001390	0.000030	0.282411	0.000010	161	0.282407	−9.4	0.5	−0.96	1.20	1.80	9.79	0.31
09BS05@09	0.001560	0.000100	0.282429	0.000010	163	0.282425	−8.8	0.5	−0.95	1.18	1.77	10.07	0.33
09BS05@10	0.001660	0.000020	0.282441	0.000020	160	0.282436	−8.4	0.6	−0.95	1.17	1.74	9.39	0.34
09BS05@11	0.000810	0.000030	0.282392	0.000010	161	0.282390	−10.0	0.5	−0.98	1.21	1.84	9.39	0.36
09BS05@12	0.001600	0.000040	0.282460	0.000010	161	0.282455	−7.7	0.5	−0.95	1.14	1.70	9.24	0.44
09BS05@13	0.001070	0.000010	0.282356	0.000010	162	0.282353	−11.3	0.5	−0.97	1.27	1.93	9.29	0.25
09BS05@14	0.001360	0.000020	0.282434	0.000010	162	0.282430	−8.6	0.5	−0.96	1.17	1.75	9.29	0.27
09BS05@15	0.001430	0.000020	0.282437	0.000010	158	0.282433	−8.5	0.5	−0.96	1.17	1.75	9.75	0.36
09BS05@16	0.001830	0.000040	0.282443	0.000010	161	0.282438	−8.3	0.5	−0.94	1.17	1.74	9.64	0.26
09BS05@17	0.002210	0.000040	0.282422	0.000010	162	0.282415	−9.1	0.5	−0.93	1.21	1.79	10.17	0.23
09BS05@18	0.001420	0.000020	0.282394	0.000010	162	0.282390	−10.0	0.5	−0.96	1.23	1.84	9.88	0.30
09BS05@19	0.001680	0.000020	0.282466	0.000020	160	0.282461	−7.5	0.6	−0.95	1.13	1.68	9.83	0.33
09BS05@20	0.001520	0.000020	0.282458	0.000020	161	0.282454	−7.7	0.6	−0.95	1.14	1.70	9.38	0.28
09BS05@21												9.67	0.27
09BS05@22												10.34	0.28
09BS05@23												9.59	0.21
Sample 09SKS-1													
09SKS-1@01	0.001600	0.000030	0.282420	0.000010	164	0.282415	−9.1	0.4	−0.95	1.20	1.79	9.04	0.27
09SKS-1@02	0.000890	0.000010	0.282414	0.000010	161	0.282411	−9.2	0.4	−0.97	1.18	1.80	9.33	0.23
09SKS-1@03	0.001260	0.000020	0.282356	0.000010	163	0.282353	−11.3	0.5	−0.96	1.27	1.93	8.79	0.35
09SKS-1@04	0.001300	0.000020	0.282406	0.000010	164	0.282402	−9.6	0.5	−0.96	1.21	1.82	8.77	0.30
09SKS-1@05	0.001450	0.000010	0.282411	0.000010	163	0.282406	−9.4	0.5	−0.96	1.20	1.81	9.11	0.23
09SKS-1@06	0.001210	0.000020	0.282431	0.000010	158	0.282427	−8.7	0.4	−0.96	1.17	1.76	9.15	0.39
09SKS-1@07	0.001410	0.000040	0.282424	0.000010	162	0.282420	−8.9	0.5	−0.96	1.18	1.78	9.18	0.32
09SKS-1@08	0.001540	0.000030	0.282384	0.000010	164	0.282379	−10.4	0.5	−0.95	1.24	1.87	11.87	0.31
09SKS-1@09	0.001330	0.000020	0.282423	0.000020	168	0.282419	−8.9	0.5	−0.96	1.18	1.78	9.36	0.27
09SKS-1@10	0.000690	0.000000	0.282412	0.000010	165	0.282410	−9.3	0.5	−0.98	1.18	1.80	9.22	0.30
09SKS-1@11	0.001520	0.000040	0.282400	0.000010	163	0.282396	−9.8	0.5	−0.95	1.22	1.83	8.87	0.40
09SKS-1@12	0.001760	0.000060	0.282416	0.000010	159	0.282411	−9.3	0.5	−0.95	1.21	1.80	9.10	0.25
09SKS-1@13	0.001640	0.000030	0.282401	0.000020	158	0.282397	−9.8	0.6	−0.95	1.22	1.83	9.73	0.38
09SKS-1@14	0.000660	0.000010	0.282280	0.000020	155	0.282278	−13.9	0.6	−0.98	1.36	2.09	9.09	0.27
09SKS-1@15	0.000900	0.000010	0.282418	0.000010	160	0.282416	−9.1	0.5	−0.97	1.17	1.79	8.96	0.46
09SKS-1@16	0.000410	0.000005	0.282280	0.000010	160	0.282279	−13.9	0.5	−0.99	1.35	2.09	9.21	0.29
09SKS-1@17	0.000670	0.000003	0.282435	0.000010	163	0.282433	−8.5	0.5	−0.98	1.14	1.75	9.21	0.29
09SKS-1@18	0.001310	0.000030	0.282423	0.000020	159	0.282419	−9.0	0.6	−0.96	1.18	1.78		
09SKS-1@19	0.001490	0.000020	0.282397	0.000010	159	0.282393	−9.9	0.5	−0.96	1.22	1.84	9.67	0.30
09SKS-1@20	0.001640	0.000040	0.282427	0.000010	162	0.282422	−8.9	0.5	−0.95	1.19	1.77	10.51	0.38
09SKS-1@21												9.12	0.28
09SKS-1@22												9.48	0.28
09SKS-1@23												8.89	0.35
09SKS-1@24												9.00	0.18
09SKS-1@25												8.93	0.34
09SKS-1@26												9.05	0.41

$\varepsilon_{Hf}(t) = 10{,}000 \times \{[(^{176}Hf/^{177}Hf)_s-(^{176}Lu/^{177}Hf)_s \times (e^{\lambda t}-1)]/[(^{176}Hf/^{177}Hf)_{CHUR(0)}-(^{176}Lu/^{177}Hf)_{CHUR} \times (e^{\lambda t}-1)]-1\}$;
$T_{DM} = 1/\lambda \times \ln\{1 + [(^{176}Hf/^{177}Hf)_s-(^{176}Hf/^{177}Hf)_{DM}]/[(^{176}Lu/^{177}Hf)_s-(^{176}Lu/^{177}Hf)_{DM}]\}$;
$T_{2DM} = T_{DM}-(T_{DM}-t) \times [(f_{cc}-f_{Lu/Hf})/(f_{cc}-f_{DM})]$, $f_{Lu/Hf} = (^{176}Lu/^{177}Hf)_s/(^{176}Lu/^{177}Hf)_{CHUR}-1$;
where f_{cc}, f_s and f_{DM} are the $f_{Lu/Hf}$ values of the continental crust, zircon sample and the depleted mantle; subscript S = analyzed zircon sample, CHUR = chondritic uniform reservoir; DM = depleted mantle; t = crystallization time of zircon; $\lambda = 1.867 \times 10^{-11}$ year^{-1}, decay constant of ^{176}Lu (Söderlund et al., 2004); $(^{176}Hf/^{177}Hf)_{DM} = 0.283250$; $(^{176}Lu/^{177}Hf)_{DM} = 0.0384$; present-day $(^{176}Hf/^{177}Hf)_{CHUR(0)} = 0.282772$; $(^{176}Lu/^{177}Hf)_{CHUR} = 0.0332$; $(^{176}Hf/^{177}Hf)_{cc} = 0.015$.

5.2. Petrogenesis

5.2.1. Crustal assimilation and magma mixing

The whole-rock $\varepsilon_{Nd}(t)$ values, two-stage Nd model ages, and zircon Hf–O isotopic compositions of the Shuikoushan and Baoshan granodiorites cannot be reproduced by modeling the effects of crustal assimilation on mantle-derived magma, or by mixing mantle-derived and crust-derived magmas (Figs. 6a and 9). In general, old crustal rocks and their derivative melts have low $\varepsilon_{Nd}(t)$ values (Ma et al., 2017, and references therein), while juvenile crustal rocks and their derivative melts have high $\varepsilon_{Nd}(t)$ values (Shen and Pan, 2013; Jiang et al., 2018, and references therein). Therefore, crustal assimilation or magma mixing during magma ascent would cause variable $\varepsilon_{Nd}(t)$ values of magmas (Shen and Pan, 2013; Ma et al., 2017, and references therein; Jiang et al., 2018, and references therein). The Shuikoushan and Baoshan granodiorites show limited variation in $\varepsilon_{Nd}(t)$ values (−7.5 to −5.1) and two-stage Nd model ages (1.38–1.57 Ga; Table 3; Wang et al., 2003a; Xie et al., 2013; Yang et al., 2016). Although there is a slightly positive correlation between SiO_2 and $\varepsilon_{Nd}(t)$ for the Shuikoushan granodiorites (Fig. 8n), this may be caused by source rocks heterogeneity rather than resulted from juvenile crustal rocks assimilation. Juvenile crustal rocks generally have zircon $\delta^{18}O$ values (5.3‰ ± 0.3‰) similar with the mantle (Huang et al., 2013, 2015a). Some assimilation of juvenile crustal rocks into the primary magma of

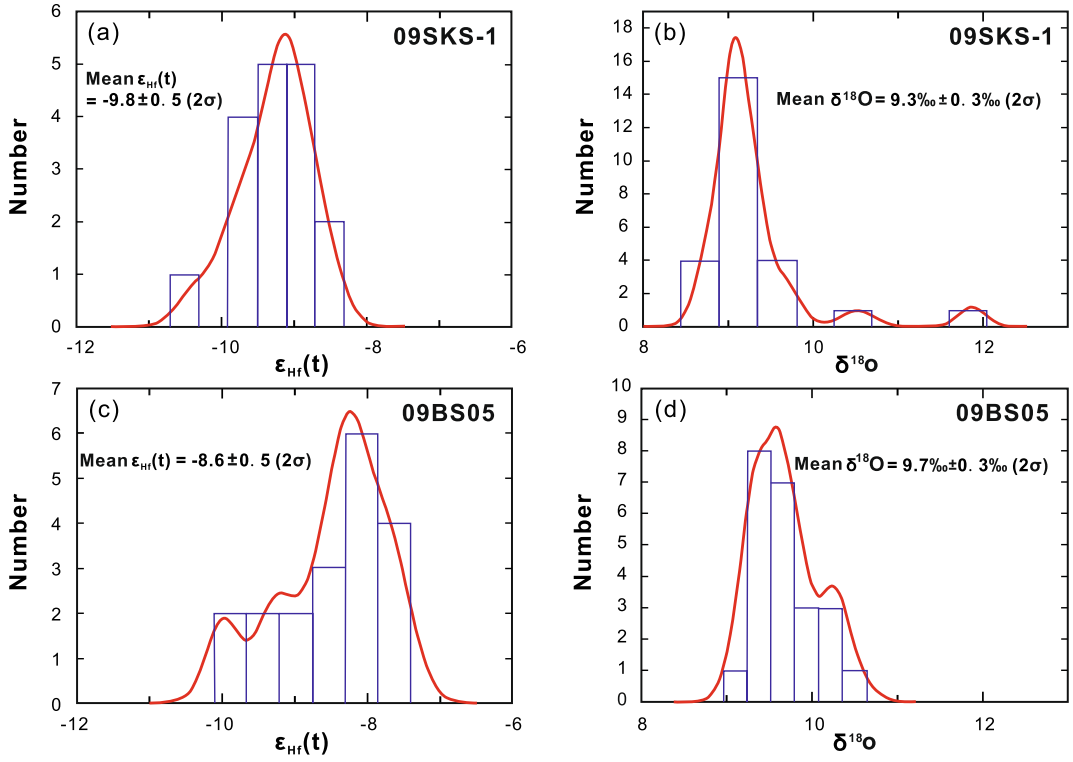

Fig. 7. (a–d) Histograms of zircon $\varepsilon_{Hf}(t)$ and $\delta^{18}O$ values from the Shuikoushan and Baoshan granodiorites.

the Shuikoushan granodiorites would cause variably higher zircon ε_{Hf} (t) and lower zircon $\delta^{18}O$ with increased SiO_2 contents (Huang et al., 2015a). This is inconsistent with relatively homogeneous zircon Hf-O isotopic compositions of the Shuikoushan and Baoshan granodiorites. The Shuikoushan and Baoshan granodiorites have relatively homogeneous zircon Hf isotopic compositions ($\varepsilon_{Hf}(t)$: −13.9 to −7.5) and $\delta^{18}O$ values (8.8‰–11.9‰; Table 4; Yang et al., 2016; Zhao et al., 2017). They have smaller variations in $\varepsilon_{Hf}(t)$ values than the Qitianling, Qianlishan, and Huashan–Guposhan granites (-15.1 to +1.5), which were suggested to be formed by mixing between mantle-derived mafic and crust-derived felsic magmas (Fig. 6b; Zhao et al., 2012; Wang et al., 2014; Chen et al., 2016). On an $\varepsilon_{Hf}(t)$ versus $\delta^{18}O$ diagram, the Shuikoushan and Baoshan granodiorites do not show a mixing trend between mafic and felsic magmas (Fig. 9).

5.2.2. Fractional crystallization

The Shuikoushan and Baoshan granodiorites have relatively wide variations of major and trace element contents, and Al_2O_3, TiO_2, $Fe_2O_3^T$, CaO, and MgO contents are negatively correlated with SiO_2 content (Fig. 10a–e). These compositional variations likely resulted from fractional crystallization where, for example, the gradual decrease in TiO_2 with increasing SiO_2 (Fig. 10b) would reflect the separation of Ti-bearing minerals such as biotite, amphibole, ilmenite and titanite. The gradual decreases in Al_2O_3, $Fe_2O_3^T$, CaO, and MgO concentrations with increasing SiO_2 content (Fig. 10a, c–e) indicate the separation of amphibole and biotite, which are enriched in these elements.

A positive correlation between $(Dy)_N/[(La)_N^{4/13}(Yb)_N^{9/13}]$ and Dy/Yb in the Shuikoushan and Baoshan granodiorites also suggests the fractionation of amphibole (Fig. 10f). Given that the $K_D(Dy)/K_D(La)$ and $K_D(Dy)/K_D(Yb)$ ratios (K_D = partition coefficient) of amphibole are greater than 1 (Sisson, 1994; Tiepolo et al., 2001), the separation of amphibole crystals can decrease Dy/Yb ratios and result in a positive linear correlation trend between $(Dy)_N/[(La)_N^{4/13}(Yb)_N^{9/13}]$ and Dy/Yb ratios in the residual magma (Davidson et al., 2012). In addition, on a chondrite-normalized rare earth element diagram (Fig. 5a), the low MREE contents compared with LREE and HREE contents also suggest the Shuikoushan and Baoshan granodiorites experienced amphibole fractionation. Sc and V are compatible in biotite (K_D values for Sc and V in biotite are 42.4 and 79.5, respectively), while, Th is incompatible in biotite (K_D value for Th in biotite is 0.01; Bea et al., 1994). Moreover, biotite has relatively high $A1_2O_3$ content (Wang et al., 2003a; Yang et al., 2016). Thus, the separation of biotite can increase SiO_2/Al_2O_3 ratios and decrease the Sc/Th and V/Th ratios in remaining magma. The separation of biotite might possibly account for negative linear correlation trends between Sc/Th or V/Th and SiO_2/Al_2O_3 in the Shuikoushan and Baoshan granodiorites (Fig. 10g-h). Given that REE are compatible in allanite (e.g. $K_D(La)$ = 2594, $K_D(Nd)$ = 1620, K_D (Sm) = 866, $K_D(Eu)$ = 111, $K_D(Yb)$ = 24.5, $K_D(Lu)$ = 33; Yang et al., 2019, and references therein), the varied REE concentrations of the Shuikoushan and Baoshan granodiorites (ΣREE = 148 to 245 ppm and 90 to 111 ppm, respectively, Table 2) suggest that they experienced the fractional crystallization of allanite. In addition, the relatively lower REE concentrations (especially LREE concentrations; Fig. 5a; Table 2) of the Baoshan granodiorites than the Shuikoushan granodiorites indicates that the former experienced higher degree of allanite fractional crystallization than the latter. Weak negative Eu anomalies suggest that plagioclase fractionation was insignificant (Fig. 5a).

5.2.3. Partial melting

The major and trace element characteristics, and whole-rock Nd and zircon Hf–O isotopic compositions of the Shuikoushan and Baoshan granodiorites suggest that the primary magma was not derived from the depleted mantle or juvenile crust. Their relatively high SiO_2 contents (58.4–70.7 wt%) and low $Mg^{\#}$ (0.28–0.54; Table 2; Wang et al., 2003a; Xie et al., 2013; Yang et al., 2016) require the removal of a significant amount of mafic minerals. However, the granodiorites do not contain the mafic minerals that commonly crystallize in mantle-derived mafic magmas, for example, augite and olivine (Fig. 2). In addition, the Shuikoushan and Baoshan granodiorites have more enriched Nd isotopic compositions ($\varepsilon_{Nd}(t)$: −7.5 to −5.1; Table 3; Wang et al., 2003a; Xie et al., 2013; Yang et al., 2016) than contemporaneous basalts from the western Nanling Range, such as the Ningyuan (+4.6 to +5.1) and

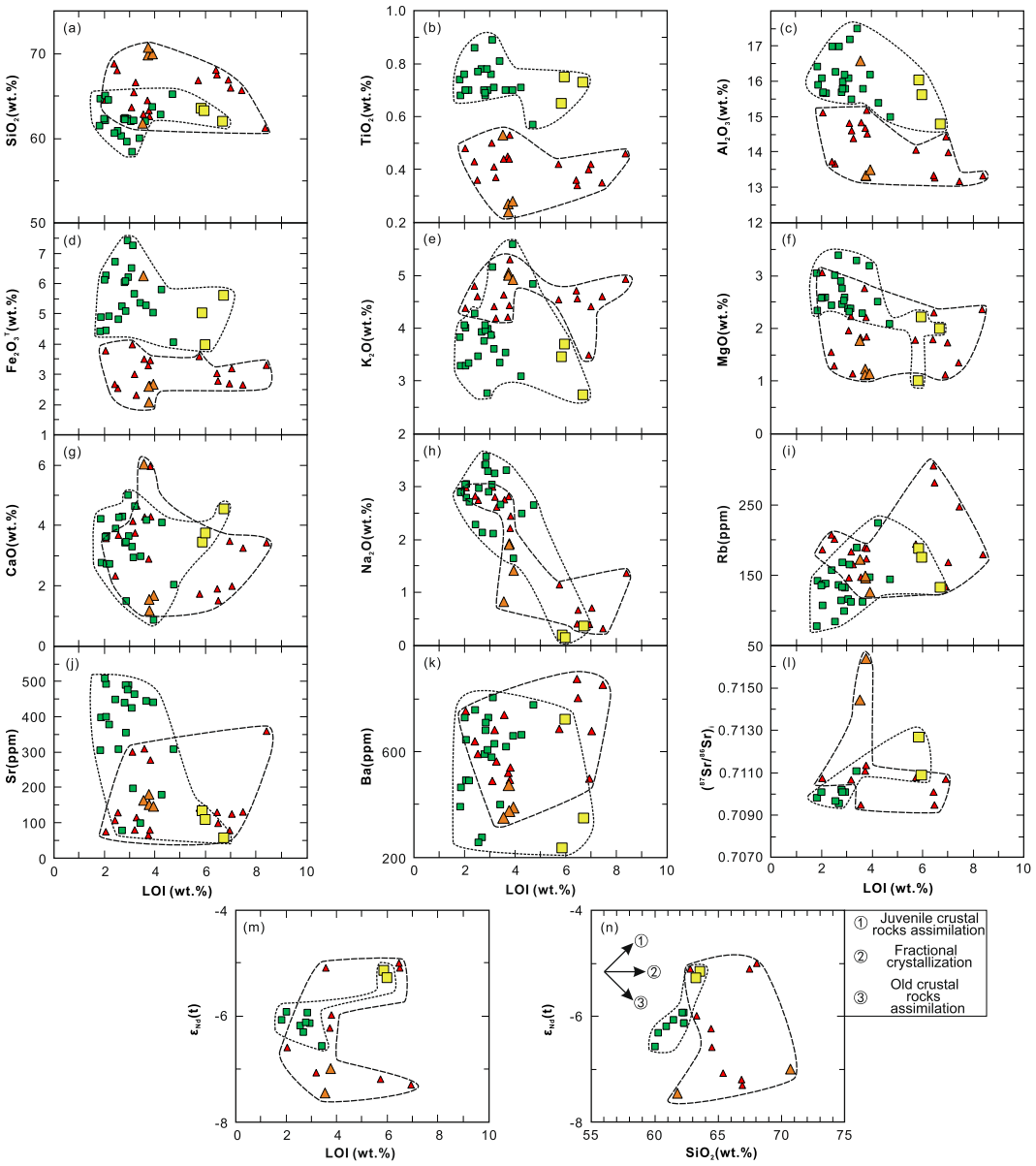

Fig. 8. (a–m) LOI (loss on ignition) vs. whole-rock major element (wt.%), selected trace element (ppm), and Sr–Nd isotopic data; (n) SiO_2 vs. $\varepsilon_{Nd}(t)$ diagrams for the Shuikoushan and Baoshan granodiorites. Data sources are as in Fig. 4.

Daoxian (−1.9 to −1.6) basalts (Li et al., 2004), as well as Middle Jurassic within-plate basalts and gabbros in the Cathaysia Block (Fig. 6a; Li et al., 2003, 2004; Wang et al., 2003b). Moreover, they also have more enriched zircon Hf isotopic compositions ($\varepsilon_{Hf}(t)$: −13.9 to −7.5) and higher zircon O isotopic compositions ($\delta^{18}O$: 8.8‰–11.9‰; Table 4; Yang et al., 2016; Zhao et al., 2017) than the enriched lithospheric mantle-derived Qinghu monzonite in the SCB ($\varepsilon_{Hf}(t)$ = +11.6; $\delta^{18}O$ = 5.4‰; Fig. 9; Li et al., 2009).

We suggest that the Shuikoushan and Baoshan granodiorites were derived by partial melting of ancient crustal source rocks. The Shuikoushan and Baoshan granodiorites have relatively low whole-rock $\varepsilon_{Nd}(t)$ and zircon $\varepsilon_{Hf}(t)$ values (−7.5 to −5.1 and −13.9 to −7.5, respectively) as well as relatively old two-stage Nd model ages (1.38–1.57 Ga; Fig. 6a–c; Tables 3 and 4). Their whole-rock $\varepsilon_{Nd}(t)$ and zircon $\varepsilon_{Hf}(t)$ values are more enriched than those of the Jurassic Qianlishan, Qitianling, and Huashan–Guposhan granites from the western Nanling Range, which have a significant mantle contribution (Zhao et al., 2012; Wang et al., 2014; Chen et al., 2016), but are similar to those of Jurassic and Triassic crustal sediment-derived granites or Neoproterozoic mafic volcaniclastic rocks and basaltic lavas in the Cathaysia Block (Fig. 6a–c; Table 5; Shen et al., 1999; Bai et al., 2007; Wang et al., 2007; Yu et al., 2007; Li et al., 2008a,b; Wang et al., 2008a; Huang et al., 2011; Wang et al., 2011a; Gao et al., 2014). Therefore, whole-rock Nd and zircon Hf isotopic compositions indicate that their source rocks were dominated by ancient crustal rock.

Magmatic zircon commonly retains the magmatic O isotope ratio (Li et al., 2009). In general, granites and diorites that are derived from a sediment-dominated source (Fig. 9; Huang et al., 2011; Jiao et al., 2015; Rong et al., 2017) or a hydrated metabasalt source (Eiler, 2001; Wang et al., 2018) will have zircon oxygen isotopic compositions of > 8.1‰. The Shuikoushan and Baoshan granodiorites have relatively high zircon $\delta^{18}O$ values (8.8‰–11.9‰ and 9.1‰–10.5‰, respectively; Fig. 7b, d; Table 4), equivalent to whole-rock values of 10.1‰–13.2‰ and 10.9‰–12.4‰ (based on the equation of Li et al., 2009, and references therein), which requires a significant contribution from supracrustal sediments or hydrated metabasalts.

However, we suggests that the crustal source of the Shuikoushan and Baoshan granodiorites may not be dominated by hydrated

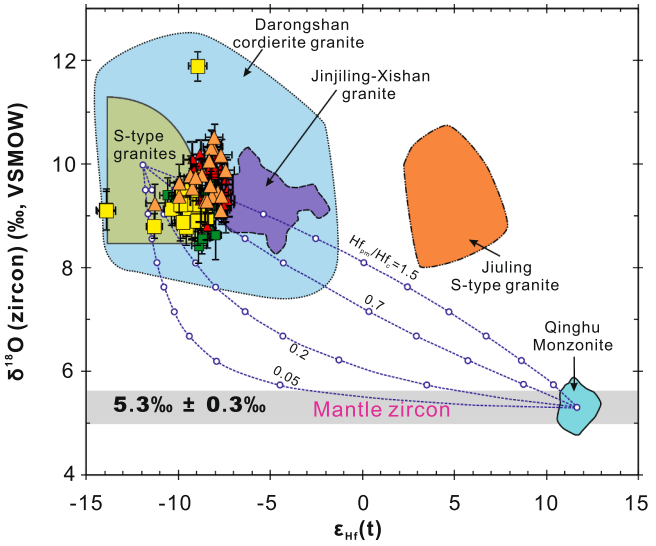

Fig. 9. Zircon Hf vs. O isotopic compositions from the Shuikoushan and Baoshan granodiorites, as well as other granitic rocks in the SCB (Qinghu, Li et al., 2009; Jinjiling–Xishan, Huang et al., 2011; Jiuling, Rong et al., 2017; Darongshan, Jiao et al., 2015), modified after Li et al. (2009). The dotted lines denote two-component mixing trends between mantle- and supracrustal-derived magmas. Hf_{pm}/Hf_c is the ratio of the Hf concentration in the parental mantle magma (pm) over crustal melt (c) for each curve, and the small open circles represent 10% mixing increments assuming mantle zircon has ε_{Hf} = +12 and $\delta^{18}O$ = 5.6‰, and supracrustal zircon has ε_{Hf} = −12 and $\delta^{18}O$ = 10‰. Zircon Hf and O isotopic compositions of the Shuikoushan and Baoshan granodiorites are from this study, Yang et al. (2016) and Zhao et al. (2017).

metabasalts. The Shuikoushan and Baoshan granodiorites have lower Cr and Ni contents (0.48–52.0 ppm and 1.79–14.7 ppm, respectively, Table 2) than the Late Archean high $\delta^{18}O$ diorites (90.4–438 ppm and 15.0–95.9 ppm, respectively) that were derived from a hydrated metabasalt source (Wang et al., 2018). In addition, the Shuikoushan and Baoshan granodiorites have more enriched Nd isotopic compositions than Paleo-Mesoproterozoic metabasaltic rocks in the Cathaysia Block basement (ε_{Nd}(161 Ma) = −0.3 to +2.2; Fig. 6a; Yuan and Wu, 1991; Jiang and Zhu, 2017, and references therein). Therefore, the Shuikoushan and Baoshan granodiorites may not be derived by partial melting of hydrated metabasalts. On the contary, they were more likely derived from crustal sediment-bearing source. This is also consistent with trace element characteristics of the Shuikoushan and Baoshan granodiorites. Because Th is relatively resistant to leaching from continental crustal sedimentary rocks during weathering (Plank and Langmuir, 1998), terrigenous clastic sediments-derived granites are enriched in Th (Wang et al., 2012). The Shuikoushan and Baoshan granodiorites are enriched in Th (13.2–16.8 ppm; Fig. 4; Table 2; Wang et al., 2003a; Xie et al., 2013; Yang et al., 2016), and their Th and Th/La ratios (0.25–0.82) are similar to metasedimentary rocks-derived Himalayan leucogranites (1.35–21.5 ppm, average: 8.73 ppm and 0.23–1.88, average: 0.77, respectively; Guo and Wilson, 2012; Huang et al., 2017a). Therefore, the trace element characteristics of the Shuikoushan and Baoshan granodiorites also suggest that they possibly originated from a continental crustal source containing metasedimentary rocks.

The Shuikoushan and Baoshan granodiorites have more depleted whole-rock Nd isotopic compositions than the Triassic and Jurassic metasedimentary rocks-derived granites (Fig. 6a). Therefore, the source material of the Shuikoushan and Baoshan granodiorites cannot be recycled Paleoproterozoic metasedimentary rocks in the Cathaysia Block, which have relatively high compositional maturity (Shen et al., 2003). On the contrary, the Middle Neoproterozoic mafic volcaniclastic rocks of the Nanhua rift basin, which consist mainly of volcanogenic metasedimentary rocks with subordinate basaltic lavas, may represent the source of the Shuikoushan and Baoshan granodiorites, since they have similar Nd isotopic compositions (Fig. 6a; Table 5). The Neoproterozoic Nanhua rift basin system in South China developed during ca. 790–760 Ma (Wang et al., 2009). The rift successions in the Cathaysia Block mainly occur at the western Nanling Range (Wang et al., 2011a, and references therein). The Nanhua rift basin was active from ca. 790 to 760 Ma, coinciding with bimodal volcanism recorded in the SCB (Wang et al., 2009, and references therein). In addition, the Middle Neoproterozoic Nanhua rift basin volcaniclastic rocks have much higher initial ε_{Nd}(t) values (maximum value is +3) than the Early Neoproterozoic Sibao Group and Late Neoproterozoic Sinian volcaniclastic rocks (maximum value is -6; Wang et al., 2011a, and references therein). Therefore, these volcaniclastic rocks were dominated by clastic material derived from the weathering of mafic volcanic rocks, with subordinate fragments of basaltic lava (Wang et al., 2011a). The Shuikoushan and Baoshan granodiorites show similar Nd isotopic compositions (-7.5 to -5.1; Table 3) to the mafic volcaniclastic rocks that are associated with sandstones and basaltic lavas in Nanhua rift basin (-8.9 to -4.1 at 161 Ma; Table 5; Li et al., 2008a,b; Wang et al., 2008a, 2011a). Given that the Shuikoushan and Baoshan granodiorites from the western Nanling Range are also located in the the Nanhua rift basin, their crustal source is most plausibly mafic volcaniclastic rocks.

In general, the mafic volcaniclastic rocks (including a large amount of juvenile mafic crustal material) contain augite, amphibole, biotite, and plagioclase phenocrysts, and basaltic or basaltic-andesite volcanic rock fragments (Rossignol et al., 2016; Ghose et al., 2017; Cavailhes and Rotevatn, 2018). Their groundmass is composed of feldspar, chlorite, calcite, and coarse lithic volcanic ash (Rossignol et al., 2016; Roverato et al., 2017). The mafic volcaniclastic rocks are hydrated and clay-poor, with low compositional maturity. During the metamorphism of mafic volcaniclastic rocks, biotite–amphibole assemblages are formed under subsolidus amphibolite-facies conditions (Clemens et al., 2011). The melting reactions that follow will initially consume both biotite and amphibole concurrently and provide the components to form a granitic magma that is in equilibrium with amphibole (Clemens et al., 2011). In contrast, clay-enriched pelites generally contain feldspar, biotite, muscovite, quartz, illite, chlorite, and ilmenite (Massonne et al., 2007; Li et al., 2016). Therefore, pelites are more enriched in aluminum and depleted in calcium than mafic volcaniclastic rocks. Felsic magma derived from the partial melting of pelites will crystallize aluminum-rich minerals, such as muscovite, cordierite, or garnet, rather than calcium-rich minerals such as amphibole (Vásquez et al., 2009).

Given that plagioclase is strongly enriched in Eu, and garnet is strongly depleted in LREE and enriched in HREE, the slightly negative Eu anomalies and the high $[La/Yb]_N$ ratios (6.0–18.2) of the Shuikoushan and Baoshan granodiorites (Fig. 5a) reflect the presence of garnet and plagioclase in their residual sources. The pressure for stability of garnet in mafic metamorphic rocks after melt extraction generally higher than 0.9 GPa (corresponding to a crustal depth of 30 km; Zhao et al., 2007, and references therein). Therefore, the Shuikoushan and Baoshan granodiorites originated at depths greater than 30 km.

5.3. Geodynamic processes

A Middle to Late Jurassic (154–162 Ma) A-type granite belt crops out in the western Nanling Range (Jiang et al., 2008; Zhao et al., 2012). The ca. 175 Ma ocean island basalt (OIB)-type Ningyuan basalts also crop out in the western Nanling Range (Wang et al., 2003b; Li et al., 2004; Zhao et al., 2012). These A-type granites and OIB-type basalts suggest that the western Nanling Range was in an extensional tectonic setting during the Middle to Late Mesozoic (175–154 Ma). All these suggest the Late Jurassic Shuikoushan and Baoshan granodiorites located in the western Nanling Rangewere also formed in a similar extensional tectonic setting. Asthenospheric mantle-derived mafic magma

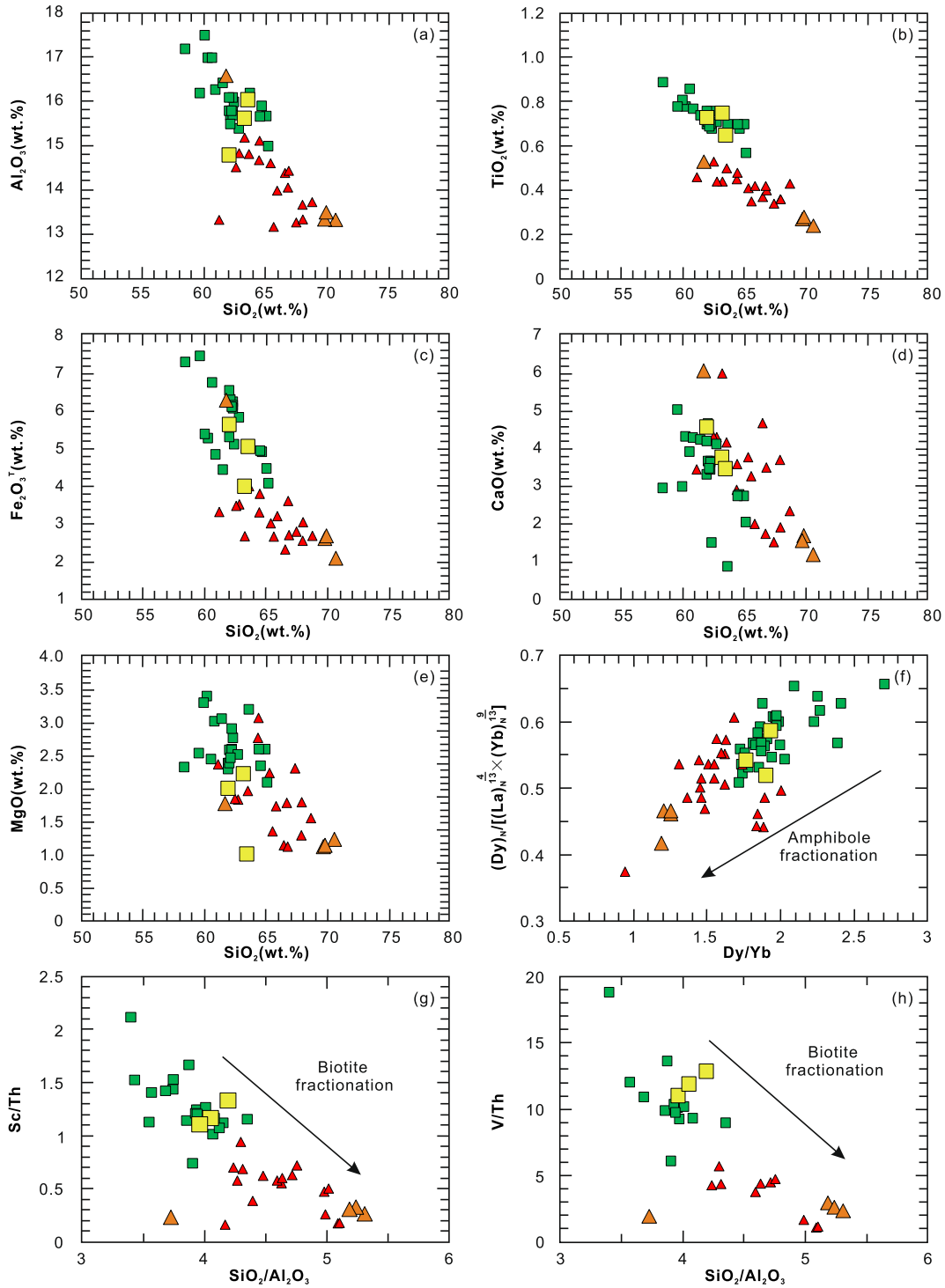

Fig. 10. (a–e) Major element oxides vs. SiO_2, (f) $(Dy)_N/[(La)_N^{4/13} \times (Yb)_N^{9/13}]$ vs. Dy/Yb, (g) Sc/Th vs. SiO_2/Al_2O_3, and (h) V/Th vs. SiO_2/Al_2O_3 diagrams for the Shuikoushan and Baoshan granodiorites. Data sources are as in Fig. 4.

may provide a heat source for the generation of the Shuikoushan and Baoshan granodiorites.

In this study, we adopt a petrogenetic model similar to that proposed by Huang et al. (2011) (Fig. 11). Roll-back of the subducted Paleo-Pacific slab caused extension of the continental crust and thinning of the continental lithosphere beneath the western Nanling Range and its surroundings (Jiang et al., 2009). Asthenospheric mantle-derived mafic magma induced the partial melting of mafic volcaniclastic rocks and produced granodioritic magma, which then ascended and was emplaced in the middle to upper crust, forming the Shuikoushan and Baoshan granodiorites (Fig. 11).

5.4. Implications

5.4.1. Petrogenesis of I-type granites

Traditionally, amphibole-bearing granites are regarded as I-type granites that were generated from crustal igneous material (Chappell and White, 1974; Gao et al., 2016). However, the high precision and spatial resolution of microanalytical isotopic techniques, such as in situ zircon O isotope analysis, reveal the petrogenesis of granites more

Table 5
Sm-Nd isotopic compositions of Nanhua Rift Basin volcaniclastic rocks, sedimentary rocks and basaltic lavas in the Cathaysia Block.

Stratigraphic unit	Samples	Lithology	Stratigraphic ages (Ga)	Nd (ppm)	Sm (ppm)	$^{147}Sm/^{144}Nd$	$^{143}Nd/^{144}Nd$	ε_{Nd} (0)	ε_{Nd} (161 Ma)	T_{2DM} (Ga)	Reference
Jiangkou Group	08SC16	Tuffaceous siltstone	0.70	37.1	7.45	0.121	0.512262	−7.3	−5.8	1.46	Wang et al. (2011a,b)
Jiangkou Group	08SC15	Tuffaceous siltstone	0.70	31.1	5.58	0.108	0.512089	−10.7	−8.9	1.53	Wang et al. (2011a,b)
Jiangkou Group	08SC14	Tuffaceous siltstone	0.70	19.6	3.51	0.109	0.512184	−8.8	−7.1	1.40	Wang et al. (2011a,b)
Yanmenzhai Formation	08SC10	Tuffaceous siltstone	0.73	40.7	8.96	0.133	0.512214	−8.3	−7.0	1.77	Wang et al. (2011a,b)
Qingshuijiang Formation	08SC32	Tuffaceous siltstone	0.78	14.4	3.72	0.156	0.512382	−5.0	−4.2	2.03	Wang et al. (2011a,b)
Qingshuijiang Formation	08SC31	Tuff	0.78	47.7	8.28	0.117	0.512291	−7.2	−4.9	1.20	Wang et al. (2011a,b)
Pinglue	08SC45	Sandstone	0.75	27.2	4.94	0.110	0.512201	−8.5	−6.8	1.39	Wang et al. (2011a,b)
Pinglue	08SC36	Sandstone	0.75	42.7	8.69	0.123	0.512114	−10.2	−8.7	1.74	Wang et al. (2011a,b)
Pinglue	08SC35	Sandstone	0.75	44.3	9.37	0.128	0.512128	−9.9	−8.6	1.81	Wang et al. (2011a,b)
Longli	08SC47	Sandstone	0.72	95.6	17.9	0.113	0.512209	−8.4	−6.7	1.43	Wang et al. (2011a,b)
Jialu	08SC66	Sandstone	0.82	95.6	17.9	0.113	0.512117	−10.2	−8.5	1.56	Wang et al. (2011a,b)
Guangfeng	03SC05-7	Basaltic lava	0.83	46.7	7.82	0.101	0.512328	−6.0	−4.1	1.12	Li et al. (2008a,b)
Guangfeng	03SC05-8	Basaltic lava	0.83	42.9	7.34	0.103	0.512292	−6.7	−4.8	1.19	Li et al. (2008a,b)
Guangfeng	03SC05-9	Basaltic lava	0.83	39.6	6.72	0.103	0.512287	−6.8	−4.9	0.98	Li et al. (2008a,b)
Bikou	05BK43	Basaltic lava	0.82	18.5	3.82	0.125	0.512125	−10.0	−8.6	1.71	Wang et al. (2008a)
Bikou	05BK44	Basaltic lava	0.82	16.7	3.86	0.139	0.512132	−9.9	−8.7	1.83	Wang et al. (2008a)
Bikou	05BK62	Basaltic lava	0.82	138	22.4	0.098	0.512301	−6.6	−4.6	1.20	Wang et al. (2008a)
Bikou	05BK75	Basaltic lava	0.82	54.8	9.41	0.104	0.512205	−8.4	−6.6	1.40	Wang et al. (2008a)

accurately. Our study suggests that the Shuikoushan and Baoshan granodiorites were mainly derived by partial melting of mafic volcaniclastic rocks. A similar example in Australia reported by Kemp et al. (2007) argued that the source of amphibole-bearing granites from the Lachlan Fold Belt of Australia contained 15%–50% supracrustal sediment. Our study, together with previous study, suggests that the amphibole-bearing granites may be derived by partial melting of mafic volcaniclastic rock-dominated source, except for partial melting of metaigneous rocks as traditional believed (Chappell and White, 1974). In addition, our study highlights compositional details that show the source sedimentary rocks of the Shuikoushan and Baoshan granodiorites were mafic volcaniclastic rocks rather than pelites. Our results show that it is prudent to consider a potential contribution from sedimentary rocks to the sources of amphibole-bearing granites, especially when those rocks have high zircon $\delta^{18}O$ values (> 8.1‰). These findings provide a new petrogenetic model for amphibole-bearing granites.

5.4.2. *Crustal reworking and Pb–Zn mineralization in South China*

The reworking and growth of the continental crust are important issues for researchers in the field of continental dynamics (Iizuka et al., 2005; Wu et al., 2006b; Zheng et al., 2007; Shu et al., 2011). Widespread Jurassic and Cretaceous granitic magmatism indicates that the SCB experienced significant Mesozoic continental reworking (Li et al., 2007; Xu et al., 2007; Jiang et al., 2009; Li et al., 2013a,b). The reworking of continental crust is evident from two observations: (1) the stratigraphic ages of global sediments are younger than their Nd model ages, suggesting that sedimentary recycling has reworked former continental crustal rocks (O'Nions et al., 1983; Condie, 2014); and (2) magmatic zircons in granitoids with elevated $\delta^{18}O$ (> 8.1‰) values were closely related to the reworking of supracrustal sediments (Wang et al., 2018, and references therein). The Shuikoushan and Baoshan granodiorites have high zircon $\delta^{18}O$ values (8.8‰–11.9‰) (Table 4), indicating that they were derived mainly by the reworking of supracrustal mafic volcaniclastic rocks that contained volcanogenic metasedimentary rocks, with subordinate basaltic lavas contributed by mafic underplating. Our study suggests that the partial melting of supracrustal metasedimentary and metaigneous rocks was an important crustal reworking mechanism in Mesozoic South China.

Pb–Zn deposits are usually associated with sedimentary rocks or sedimentary rocks-derived granites (Leach et al., 2010; Zhao et al., 2016; Xu et al., 2018). The field relationships, ages, and S and Pb isotopic compositions of the Shuikoushan and Baoshan Pb–Zn ores suggest that mineralization was genetically related to the granodiorites (Lu et al., 2006, 2013; Huang et al., 2015b; Xie et al., 2015; Ding et al., 2016). However, the Shuikoushan and Baoshan granodiorites contain amphibole (this study; Wang et al., 2003a; Zuo et al., 2014a; Zhao et al., 2017). Traditionally, amphibole-bearing granites are considered to be I-type granites, derived by partial melting of crustal igneous rocks (Chappell and White, 1974, 2001). Our findings that the source of the Shuikoushan and Baoshan granodiorites was dominated by metasedimentary rocks have novel metallogenic implications. The Pb–Zn mineralization occurs mainly in fractures between the sedimentary host rocks and the granodiorite, and is spatially, temporally and genetically related to the host granodiorite intrusions (Huang et al., 2015b). Accordingly, the source of the Pb–Zn ores is ultimately linked to metasedimentary rock sources associated with the Shuikoushan and Baoshan granodiorites. Therefore, we suggest that granodiorites generated by the partial melting of crustal metasedimentary and metaigneous rocks favor Pb–Zn mineralization.

6. Conclusions

(1) LA–ICP–MS zircon U–Pb ages show that the Shuikoushan and Baoshan granodiorites in the western Nanling Range of South China were formed during the Late Jurassic (ca. 161 Ma).

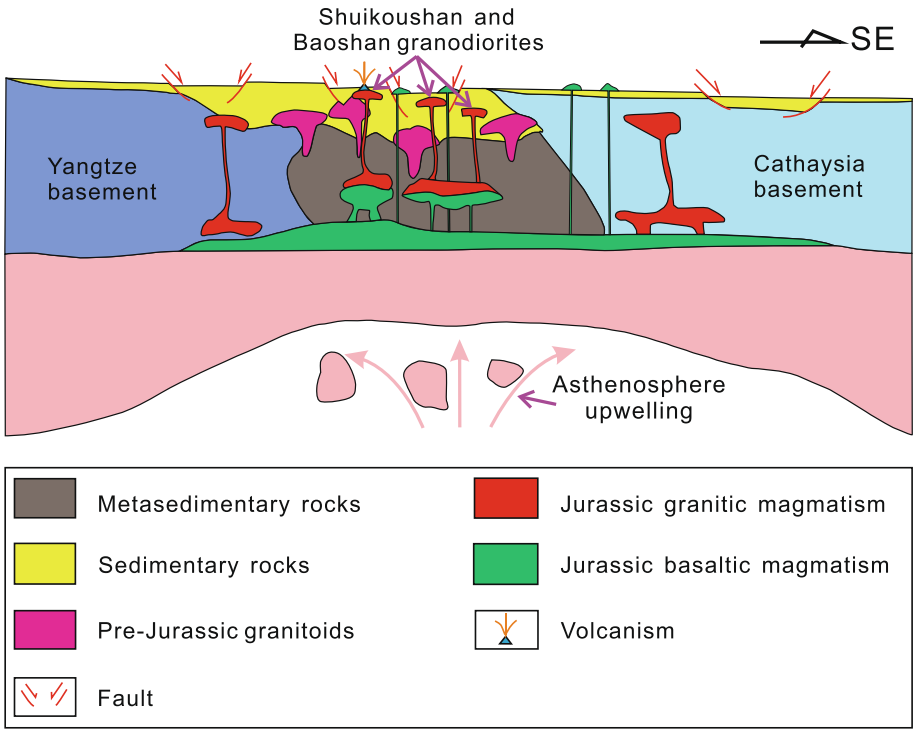

Fig. 11. Petrogenetic model for the Shuikoushan and Baoshan granodiorites (modified from Huang et al., 2011). Mafic magma derived from asthenospheric mantle material ascended and was emplaced in the middle to lower crust. The mafic magma caused the partial melting of mafic volcaniclastic rocks. The partial melting generated the Shuikoushan and Baoshan granodioritic magma, which ascended and was emplaced in the middle to upper crust, forming the Shuikoushan and Baoshan granodiorites. Not to scale.

(2) The source material of the Shuikoushan and Baoshan granodiorites was mainly Middle Neoproterozoic mafic volcaniclastic rocks from the lower crust of the Nanhua rift basin, South China.
(3) The partial melting of crustal metasedimentary and metaigneous rocks appears to be an important crustal reworking mechanism in Mesozoic South China, and granodiorites generated by such a mechanism might favor Pb–Zn mineralization.

CRediT authorship contribution statement

Xiao Liu: Conceptualization, Data curation, Formal analysis, Investigation, Visualization, Writing - original draft. **Qiang Wang:** Conceptualization, Data curation, Funding acquisition, Project administration, Investigation, Resources, Supervision, Writing - review & editing. **Lin Ma:** Conceptualization, Project administration, Visualization, Writing - review & editing. **Derek A. Wyman:** Investigation, Writing - review & editing. **Zhen-Hua Zhao:** Conceptualization, Investigation. **Jin-Hui Yang:** Resources. **Feng Zi:** Investigation. **Gong-Jian Tang:** Conceptualization, Software, Writing - review & editing. **Wei Dan:** Conceptualization, Software, Writing - review & editing. **Jin-Sheng Zhou:** Conceptualization, Visualization, Writing - review & editing.

Declaration of Competing Interest

The authors declare that they have no known competing financial interests or personal relationships that could have appeared to influence the work reported in this paper.

Acknowledgements

We are very grateful for the hard work of editor-in chief Professor Mei-Fu Zhou, handing editor Professor Xiao-Lei Wang, Professor Jin-Hai Yu and Doctor Peng Gao, whose constructive criticism and suggestions have improved this paper significantly. We appreciate the assistance of Ying Liu and Lin-Li Chen for major element analyses and zircon cathodoluminescence imaging, and Xiang-Lin Tu, Guang-Qian Hu, Xi-Rong Liang, Zhong-Yuan Ren, and Jin-Long Ma for whole-rock geochemical analyses. We also thank Guo-Ning Gou, Lu-Lu Hao, and Quan Ou for their help with U–Pb age analyses. Thanks to Jun Wang, Wan-Long Hu and Zong-Yong Yang for their help to improve this manuscript. Financial support was provided by the National Key Research and Development Program of China (Grant number: 2016YFC0600407), the Key Program of the Chinese Academy of Sciences (Grant number: QYZDJ–SSW–DQC026), the National Natural Science Foundation of China (Grant number: 41630208), the Key Program of Guangzhou City (Grant number: No. 201707020032), the Youth Innovation Promotion Association CAS (2017404) and Guangzhou Institute of Geochemistry, Chinese Academy of Sciences (GIG–CAS) 135 project number 135TP201601. This is contribution IS–2809 from GIG–CAS.

Appendix A. Supplementary material

Supplementary data to this article can be found online at https://doi.org/10.1016/j.jseaes.2020.104236.

References

Bai, D.Y., Zhou, L., Ma, T.Q., Wang, X.H., 2007. Genesis and tectonic setting of Indosinian granites in southeast Hunan. Acta Petrologica et Mineralogica 26, 197–212 (in Chinese with English abstract).
Bea, F., Pereira, M.D., Stroh, A., 1994. Mineral/leucosome trace-element partitioning in a peraluminous migmatite (a laser ablation-ICP-MS study). Chem. Geol. 117, 291–312.
Cavailhes, T., Rotevatn, A., 2018. Deformation bands in volcaniclastic rocks-Insights from the Shihtiping tuffs, Coastal Range of Taiwan. J. Struct. Geol. 113, 155–175.
Chappell, B.W., White, A.J.R., 1974. Two contrasting granite types. Pac. Geol. 8, 173–174.
Chappell, B.W., White, A.J.R., 2001. Two contrasting granite types: 25 years later. Aust. J. Earth Sci. 48, 489–499.
Chauvel, C., Lewin, E., Carpentier, M., Arndt, N.T., Marini, J.C., 2008. Role of recycled oceanic basalt and sediment in generating the Hf-Nd mantle array. Nat. Geosci. 1, 64–67.
Chen, J.F., Jahn, B.M., 1998. Crustal evolution of southeastern China: Nd and Sr isotopic evidence. Tectonophysics 284, 101–133.
Chen, D., Liu, J.Y., Wang, X.H., Yang, J., Ma, T.Q., Luo, L., 2017. The petrogeochemistry, SHRIMP zircon U-Pb age, and Hf isotope Character of Wufengxian Pluton in Hunan Province. Geol. Sci. Technol. Inf. 36, 1–12 (in Chinese with English abstract).
Chen, Y.X., Li, H., Sun, W.D., Ireland, T., Tian, X.F., Hu, Y.B., Yang, W.B., Chen, C., Xu, D.R., 2016. Generation of Late Mesozoic Qianlishan A2-type granite in Nanling Range, South China: implications for Shizhuyuan W-Sn mineralization and tectonic

evolution. Lithos 266, 435–452.
Clemens, J.D., Stevens, G., Farina, F., 2011. The enigmatic sources of I-type granites: the peritectic connexion. Lithos 126, 174–181.
Condie, K.C., 2014. Growth of continental crust: a balance between preservation and recycling. Mineral. Mag. 78, 623–638.
Davidson, J., Turner, S., Plank, T., 2012. Dy/Dy*: variations arising from mantle sources and petrogenetic processes. J. Petrol. 54, 525–537.
DePaolo, D.J., 1981. A neodymium and strontium isotopic study of the Mesozoic calc-alkaline granitic batholiths of the Sierra Nevada and Peninsular Ranges, California. J. Geophys. Res. Solid Earth 86, 10470–10488.
Ding, T., Ma, D.S., Lu, J.J., Zhang, R.Q., Xie, Y.C., 2016. Sulfur and lead isotopic compositions of granodiorites and fluid inclusions in Baoshan deposit, Hunan Province. Mineral Deposits 35, 663–676.
Eiler, J.M., 2001. Oxygen isotope variations of basaltic lavas and upper mantle rocks. Rev. Mineral. Geochem. 43, 319–364.
Fu, J.M., Ma, C.Q., Xie, C.F., Zhang, Y.M., Peng, S.B., 2004. The determination of the formation ages of the Xishan volcanic-intrusive complex in southern Hunan province. Acta Geoscientica Sinica 25, 303–308 (in Chinese with English abstract).
Gao, P., Zhao, Z.F., Zheng, Y.F., 2014. Petrogenesis of Triassic granites from the Nanling Range in South China: implications for geochemical diversity in granites. Lithos 210–211, 40–56.
Gao, P., Zheng, Y.F., Zhao, Z.F., 2016. Experimental melts from crustal rocks: a lithochemical constraint on granite petrogenesis. Lithos 266, 133–157.
Ghose, N.C., Chatterjee, N., Windley, B.F., 2017. Subaqueous early eruptive phase of the late Aptian Rajmahal volcanism, India: Evidence from volcaniclastic rocks, bentonite, black shales, and oolite. Geosci. Front. 8, 809–822.
Gilder, S.A., Gill, J., Coe, R.S., Zhao, X., Liu, Z., Wang, G., Yuan, K., Liu, W., Kuang, G., Wu, H., 1996. Isotopic and paleomagnetic constraints on the Mesozoic tectonic evolution of south China. J. Geophys. Res. Solid Earth 101, 16137–16154.
Griffin, W.L., Pearson, N.J., Belousova, E., Jackson, S.E., Van Achterbergh, E., O'Reilly, S.Y., Shee, S.R., 2000. The Hf isotope composition of cratonic mantle: LAM-MC-ICPMS analysis of zircon megacrysts in kimberlites. Geochim. Cosmochim. Acta 64, 133–147.
Guo, Z.F., Wilson, M., 2012. The Himalayan leucogranites: constraints on the nature of their crustal source region and geodynamic setting. Gondwana Res. 22, 360–376.
Hastie, A.R., Kerr, A.C., Pearce, J.A., Mitchell, S.F., 2007. Classification of altered volcanic island arc rocks using immobile trace elements: development of the Th-Co discrimination diagram. J. Petrol. 48, 2341–2357.
He, Z.Y., Xu, X.S., Niu, Y.L., 2010. Petrogenesis and tectonic significance of a Mesozoic granite-syenite-gabbro association from inland South China. Lithos 119, 621–641.
Hoskin, P., Black, L., 2000. Metamorphic zircon formation by solid-state recrystallization of protolith igneous zircon. J. Metamorph. Geol. 18, 423–439.
Hu, Z.C., Liu, Y.S., Gao, S., Liu, W.G., Zhang, W., Tong, X.R., Lin, L., Zong, K.Q., Li, M., Chen, H.H., Zhou, L., Yang, L., 2012. Improved in situ Hf isotope ratio analysis of zircon using newly designed X skimmer cone and jet sample cone in combination with the addition of nitrogen by laser ablation multiple collector ICP-MS. J. Anal. At. Spectrom. 27, 1391–1399.
Huang, C.M., Zhao, Z.D., Li, G.M., Zhu, D.C., Liu, D., Shi, Q.S., 2017a. Leucogranites in Lhozag, southern Tibet: Implications for the tectonic evolution of the eastern Himalaya. Lithos 294, 246–262.
Huang, H.Q., Li, X.H., Li, W.X., Li, Z.X., 2011. Formation of high $\delta^{18}O$ fayalite-bearing A-type granite by high-temperature melting of granulitic metasedimentary rocks, southern China. Geology 39, 903–906.
Huang, H.Q., Li, X.H., Li, Z.X., Li, W.X., 2013. Intraplate crustal remelting as the genesis of Jurassic high-K granites in the coastal region of the Guangdong Province, SE China. J. Asian Earth Sci. 74, 280–302.
Huang, H.Q., Li, X.H., Li, Z.X., Li, W.X., 2015a. Formation of the Jurassic South China Large Granitic Province: insights from the genesis of the Jiufeng pluton. Chem. Geol. 401, 43–58.
Huang, J.C., Peng, J.T., Yang, J.H., Zhang, B.L., Xu, C.X., 2015b. Precise zircon U-Pb and molybdenite Re-Os dating of the Shuikoushan granodiorite-related Pb-Zn mineralization, southern Hunan, South China. Ore Geol. Rev. 71, 305–317.
Huang, X.D., Lu, J.J., Sizaret, S., Wang, R.C., Ma, D.S., Zhang, R.Q., Zhao, X., Wu, J.W., 2017b. Petrogenetic differences between the Middle-Late Jurassic Cu-Pb-Zn-bearing and W-bearing granites in the Nanling Range, South China: A case study of the Tongshanling and Weijia deposits in southern Hunan Province. Sci. China Earth Sci. 60, 1220–1236.
Iizuka, T., Hirata, T., Komiya, T., Rino, S., Katayama, I., Motoki, A., Maruyama, S., 2005. U-Pb and Lu-Hf isotope systematics of zircons from the Mississippi River sand: Implications for reworking and growth of continental crust. Geology 33, 485–488.
Jiang, D.S., Xu, X.S., Xia, Y., Erdmann, S., 2018. Magma mixing in a granite and related rock association: Insight from its mineralogical, petrochemical, and "reversed isotope" features. J. Geophys. Res. Solid Earth 123, 2262–2285.
Jiang, S.Y., Zhao, K.D., Jiang, Y.H., Dai, B.Z., 2008. Characteristics and genesis of Mesozoic A-type granites and associated mineral deposits in the Southern Hunan and Northern Guangxi Provinces along the Shi-Hang Belt, South China. Geol. J. China Univ. 14, 496–509 (in Chinese with English abstract).
Jiang, Y.H., Jiang, S.Y., Dai, B.Z., Liao, S.Y., Zhao, K.D., Ling, H.F., 2009. Middle to late Jurassic felsic and mafic magmatism in southern Hunan province, southeast China: Implications for a continental arc to rifting. Lithos 107, 185–204.
Jiang, Y.H., Zhu, S.Q., 2017. Petrogenesis of the Late Jurassic peraluminous biotite granites and muscovite-bearing granites in SE China: geochronological, elemental and Sr–Nd–O–Hf isotopic constraints. Contrib. Miner. Petrol. 172, 1–27.
Jiao, S.J., Li, X.H., Huang, H.Q., Deng, X.G., 2015. Metasedimentary melting in the formation of charnockite: Petrological and zircon U-Pb-Hf-O isotope evidence from the Darongshan S-type granitic complex in southern China. Lithos 239, 217–233.
Kemp, A.I.S., Hawkesworth, C.J., Foster, G.L., Paterson, B.A., Woodhead, J.D., Hergt, J.M., Gray, C.M., Whitehouse, M.J., 2007. Magmatic and crustal differentiation history of granitic rocks from Hf-O isotopes in zircon. Science 315, 980–983.
Leach, D.L., Bradley, D.C., Huston, D., Pisarevsky, S.A., Taylor, R.D., Gardoll, S.J., 2010. Sediment-hosted lead-zinc deposits in Earth history. Econ. Geol. 105, 593–625.
Li, W.X., Li, X.H., Li, Z.X., 2008a. Middle Neoproterozoic syn-rifting volcanic rocks in Guangfeng, South China: petrogenesis and tectonic significance. Geol. Mag. 145, 475–489.
Li, X.H., Chen, Z.G., Liu, D.Y., Li, W.X., 2003. Jurassic gabbro-granite-syenite suites from Southern Jiangxi Province, SE China: age, origin, and tectonic significance. Int. Geol. Rev. 45, 898–921.
Li, X.H., Chung, S.L., Zhou, H., Lo, C.H., Liu, Y., Chen, C.H., 2004. Jurassic intraplate magmatism in southern Hunan-eastern Guangxi: $^{40}Ar/^{39}Ar$ dating, geochemistry, Sr-Nd isotopes and implications for the tectonic evolution of SE China. Geol. Soc., London, Spec. Publ. 226, 193–215.
Li, X.H., Li, W.X., Li, Q.L., Wang, X.C., Liu, Y., Yang, Y.H., 2010a. Petrogenesis and tectonic significance of the ~850 Ma Gangbian alkaline complex in South China: evidence from in situ zircon U-Pb dating, Hf-O isotopes and whole-rock geochemistry. Lithos 114, 1–15.
Li, X.H., Li, W.X., Li, Z.X., 2007. On the genetic classification and tectonic implications of the Early Yanshanian granitoids in the Nanling Range, South China. Chin. Sci. Bull. 52, 1873–1885.
Li, X.H., Li, W.X., Wang, X.C., Li, Q.L., Liu, Y., Tang, G.Q., 2009. Role of mantle-derived magma in genesis of early Yanshanian granites in the Nanling Range, South China: in situ zircon Hf-O isotopic constraints. Sci. China, Ser. D Earth Sci. 52, 1262–1278.
Li, X.H., Li, Z.X., Li, W.X., Wang, X.C., Gao, Y.Y., 2013a. Revisiting the "C-type adakites" of the Lower Yangtze River Belt, central eastern China: in-situ zircon Hf-O isotope and geochemical constraints. Chem. Geol. 345, 1–15.
Li, X.H., Long, W.G., Li, Q.L., Liu, Y., Zheng, Y.F., Yang, Y.H., Chamberlain, K.R., Wan, D.F., Guo, C.H., Wang, X.C., 2010b. Penglai zircon megacrysts: a potential new working reference material for microbeam determination of Hf-O isotopes and U-Pb age. Geostand. Geoanal. Res. 34, 117–134.
Li, X.H., Tang, G.Q., Gong, B., Yang, Y.H., Hou, K.J., Hu, Z.C., Li, Q.L., Liu, Y., Li, W.H., 2013b. Qinghu zircon: A working reference for microbeam analysis of U-Pb age and Hf and O isotopes. Chin. Sci. Bull. 58, 4647–4654.
Li, X.H., Zhou, H., Chung, S.L., Lo, C.H., Wei, G., Liu, Y., Lee, C.Y., 2002. Geochemical and Sr-Nd isotopic characteristics of late Paleogene ultrapotassic magmatism in southeastern Tibet. Int. Geol. Rev. 44, 559–574.
Li, Y., Zhang, Y.Q., Su, J.B., Li, J.H., Dong, S.W., 2015. Zircon U-Pb dating of Dayishan and Tashan Plutons in Hunan Province and its tectonic implications. Acta Geoscientica Sinica 36, 303–312 (in Chinese with English abstract).
Li, Y.H., Zheng, J.P., Xiong, Q., Wang, W., Ping, X.Q., Li, X.Y., Tang, H.Y., 2016. Petrogenesis and tectonic implications of Paleoproterozoic metapelitic rocks in the Archean Kongling Complex from the northern Yangtze Craton, South China. Precambr. Res. 276, 158–177.
Li, Z.X., Bogdanova, S.V., Collins, A.S., Davidson, A., De Waele, B., Ernst, R.E., Fitzsimons, I.C.W., Fuck, R.A., Gladkochub, D.P., Jacobs, J., Karlstrom, K.E., Lu, S., Natapov, L.M., Pease, V., Pisarevsky, S.A., Thrane, K., Vernikovsky, V., 2008b. Assembly, configuration, and break-up history of Rodinia: a synthesis. Precambr. Res. 160, 179–210.
Liang, X.R., Wei, G.J., Li, X.H., Liu, Y., 2003. Precise measurement of $^{143}Nd/^{144}Nd$ and Sm/Nd ratios using multiple-collectors inductively coupled plasma-mass spectrometer (MC-ICPMS). Geochimica 32, 91–96 (in Chinese with English abstract).
Liu, Y.S., Hu, Z.C., Gao, S., Günther, D., Xu, J., Gao, C.G., Chen, H.H., 2008. In situ analysis of major and trace elements of anhydrous minerals by LA-ICP-MS without applying an internal standard. Chem. Geol. 257, 34–43.
Lu, R., Xu, Z.W., Lu, J.J., Wang, R.C., Zuo, C.H., Zhao, Z.X., Miao, B.H., 2013. Genesis of the Shuikoushan lead-zinc deposit, Changning City, Hunan Province. J. Nanjing Univ. (Nat. Sci.) 49, 732–746 (in Chinese with English abstract).
Lu, Y.F., Ma, L.Y., Qu, W.J., Mei, Y.P., Chen, X.Q., 2006. U-Pb and Re-Os isotope geochronology of Baoshan Cu-Mo polymetallic ore deposit in Hunan Province. Acta petrologica sinica 22, 2483–2492 (in Chinese with English abstract).
Ludwig, K.R., 2012. Isoplot 3.75: A Geochronological Toolkit for Microsoft Excel: Berkeley Geochronology Center Special Publication 5, pp. 1–75.
Ma, L., Wang, Q., Kerr, A.C., Yang, J.H., Xia, X.P., Ou, Q., Yang, Z.Y., Sun, P., 2017. Paleocene (ca. 62 Ma) Leucogranites in Southern Lhasa, Tibet: Products of Syn-collisional Crustal Anatexis during Slab Roll-back? J. Petrol. 58, 2089–2114.
Massonne, H.J., Willner, A.P., Gerya, T., 2007. Densities of metapelitic rocks at high to ultrahigh pressure conditions: What are the geodynamic consequences? Earth Planet. Sci. Lett. 256, 12–27.
Morel, M.L.A., Nebel, O., Nebel-Jacobsen, Y.J., Miller, J.S., Vroon, P.Z., 2008. Hafnium isotope characterization of the GJ-1 zircon reference material by solution and laser-ablation MC-ICPMS. Chem. Geol. 255, 231–235.
O'Nions, R.K., Hamilton, P.J., Hooker, P.J., 1983. A Nd isotope investigation of sediments related to crustal development in the British Isles. Earth Planet. Sci. Lett. 63, 229–240.
Plank, T., Langmuir, C.H., 1998. The chemical composition of subducting sediment and its consequences for the crust and mantle. Chem. Geol. 145, 325–394.
Qiu, R.Z., Deng, J.F., Cai, Z.Y., Zhou, S., Chang, H.L., Du, S.H., 2003. Nd isotopic characteristics and genesis of Xianghualing 430 granitic body, Hunan Province. Acta Petrologica et Mineralogica 22, 42–46 (in Chinese with English abstract).
Quan, T.J., Kong, H., Fei, L.D., Wang, G., Li, H., Wu, C.M., 2012. Petrogenesis of granodiorite porphyry in Baoshan deposit: Constraints from geochemistry, zircon U-Pb chronology and Hf isotopes. Chin. J. Nonferrous Met. 22, 611–621 (in Chinese with English abstract).
Richards, A., Argles, T., Harris, N., Parrish, R., Ahmad, T., Darbyshire, F., Draganits, E.,

2005. Himalayan architecture constrained by isotopic tracers from clastic sediments. Earth Planet. Sci. Lett. 236, 773–796.
Rong, W., Zhang, S.B., Zheng, Y.F., 2017. Back-reaction of peritectic garnet as an explanation for the origin of mafic enclaves in S-type Granite from the Jiuling Batholith in South China. J. Petrol. 58, 569–598.
Rossignol, C., Bourquin, S., Poujol, M., Hallot, E., Dabard, M.P., Nalpas, T., 2016. The volcaniclastic series from the luang prabang basin, Laos: A witness of a triassic magmatic arc? J. Asian Earth Sci. 120, 159–183.
Roverato, M., Juliani, C., Dias-Fernandes, C.M., Capra, L., 2017. Paleoproterozoic andesitic volcanism in the southern Amazonian craton, the Sobreiro Formation: new insights from lithofacies analysis of the volcaniclastic sequences. Precambr. Res. 289, 18–30.
Rudnick, R.L., Gao, S., 2003. Composition of the continental crust. In: Rudnick, R.L. (Ed.), The Crust, Treatise in Geochemistry. Elsevier, New York, pp. 1–64.
Shen, P., Pan, H., 2013. Country-rock contamination of magmas associated with the Baogutu porphyry Cu deposit, Xinjiang, China. Lithos 177, 451–469.
Shen, W.Z., Ling, H.F., Li, W.X., Wang, D.Z., Huang, X., Pan, J., 1999. Nd-Sr isotopic study of Mesozoic granitoids in Jiangxi Province. Chin. Sci. Bull. 44, 1427–1431.
Shen, W.Z., Yu, J.H., Zhao, L., Chen, Z.L., Lin, H.C., 2003. Nd isotopic characteristics of post-Archean sediments from the Eastern Nanling Range: Evidence for crustal evolution. Chin. Sci. Bull. 48, 1679–1685.
Shu, X.J., Wang, X.L., Sun, T., Xu, X., Dai, M.N., 2011. Trace elements, U-Pb ages and Hf isotopes of zircons from Mesozoic granites in the western Nanling Range, South China: implications for petrogenesis and W-Sn mineralization. Lithos 127, 468–482.
Sisson, T.W., 1994. Hornblende-melt trace-element partitioning measured by ion microprobe. Chem. Geol. 117, 331–344.
Söderlund, U., Patchett, P.J., Vervoort, J.D., Isachsen, C.E., 2004. The ^{176}Lu decay constant determined by Lu-Hf and U-Pb isotope systematics of Precambrian mafic intrusions. Earth Planet. Sci. Lett. 219, 311–324.
Sun, S.-S., McDonough, W.F., 1989. Chemical and isotopic systematics of oceanic basalts: implications for mantle composition and processes. Geol. Soc., London, Spec. Publ. 42, 313–345.
Sun, T., 2006. A new map showing the distribution of granites in South China and its explanatory notes. Geol. Bull. China 25, 332–335 (in Chinese with English abstract).
Tiepolo, M., Bottazzi, P., Foley, S.F., Oberti, R., Vannucci, R., Zanetti, A., 2001. Fractionation of Nb and Ta from Zr and Hf at mantle depths: the role of titanian pargasite and kaersutite. J. Petrol. 42, 221–232.
Vásquez, P., Glodny, J., Franz, G., Romer, R.L., Gerdes, A., 2009. Origin of fayalite granitoids: New insights from the Cobquecura Pluton, Chile, and its metapelitic xenoliths. Lithos 110, 181–198.
Wang, D., Guo, J.H., Qian, Q., Fu, B., 2018. Formation of Late Archean high-δ^{18}O diorites through partial melting of hydrated metabasalts. J. Petrol. 59, 419–445.
Wang, Q., Xu, J.F., Jian, P., Bao, Z.W., Zhao, Z.H., Li, C.F., Xiong, X.L., Ma, J.L., 2006. Petrogenesis of adakitic porphyries in an extensional tectonic setting, Dexing, South China: implications for the genesis of porphyry copper mineralization. J. Petrol. 47, 119–144.
Wang, Q., Chung, S.L., Li, X.H., Derek, W., Li, Z.X., Sun, W.D., Qiu, H.N., Liu, Y.S., Zhu, Y.T., 2012. Crustal melting and flow beneath northern Tibet: evidence from Mid-Miocene to Quaternary strongly peraluminous rhyolites in the southern Kunlun range. J. Petrol. 53, 2523–2566.
Wang, X.C., Li, X.H., Li, W.X., Li, Z.X., 2009. Variable involvements of mantle plumes in the genesis of mid-Neoproterozoic basaltic rocks in South China: a review. Gondwana Res. 15, 381–395.
Wang, X.C., Li, X.H., Li, W.X., Li, Z.X., Liu, Y., Yang, Y.H., Liang, X.R., Tu, X.L., 2008a. The Bikou basalts in the northwestern Yangtze block, South China: Remnants of 820–810 Ma continental flood basalts? Geol. Soc. Am. Bull. 120, 1478–1492.
Wang, X.C., Li, Z.X., Li, X.H., Li, Q.L., Zhang, Q.R., 2011a. Geochemical and Hf-Nd isotope data of Nanhua rift sedimentary and volcaniclastic rocks indicate a Neoproterozoic continental flood basalt provenance. Lithos 127, 427–440.
Wang, Y.J., Fan, W.M., Cawood, P.A., Li, S.Z., 2008b. Sr-Nd-Pb isotopic constraints on multiple mantle domains for Mesozoic mafic rocks beneath the South China Block hinterland. Lithos 106, 297–308.
Wang, Y.J., Fan, W.M., Guo, F., 2003a. Geochemistry of early Mesozoic potassium-rich diorites-granodiorites in southeastern Hunan Province, South China: Petrogenesis and tectonic implications. Geochem. J. 37, 427–448.
Wang, Y.J., Fan, W.M., Guo, F., Peng, T.P., Li, C.W., 2003b. Geochemistry of mesozoic mafic rocks adjacent to the Chenzhou-Linwu fault, South China: implications for the lithospheric boundary between the Yangtze and Cathaysia blocks. Int. Geol. Rev. 45, 263–286.
Wang, Y.J., Fan, W.M., Sun, M., Liang, X.Q., Zhang, Y.H., Peng, T.P., 2007. Geochronological, geochemical and geothermal constraints on petrogenesis of the Indosinian peraluminous granites in the South China Block: a case study in the Hunan Province. Lithos 96, 475–502.
Wang, Y.J., Zhang, A.M., Fan, W.M., Zhao, G.C., Zhang, G.W., Zhang, Y.Z., Zhang, F.F., Li, S.Z., 2011b. Kwangsian crustal anatexis within the eastern South China Block: geochemical, zircon U-Pb geochronological and Hf isotopic fingerprints from the gneissoid granites of Wugong and Wuyi-Yunkai Domains. Lithos 127, 239–260.
Wang, Z.Q., Chen, B., Ma, X.H., 2014. Petrogenesis of the Late Mesozoic Guposhan composite plutons from the Nanling Range, South China: Implications for W-Sn mineralization. Am. J. Sci. 314, 235–277.
Wei, G.J., Liang, X.R., Li, X.H., Liu, Y., 2002. Precise measurement of Sr isotopic composition of liquid and solid base using (LP) MC-ICPMS. Geochimica 31, 295–299 (in Chinese with English abstract).
Winchester, J.A., Floyd, P.A., 1977. Geochemical discrimination of different magma series and their differentiation products using immobile elements. Chem. Geol. 20, 325–343.
Wu, F.Y., Li, X.H., Yang, J.H., Zheng, Y.F., 2007a. Discussions on the petrogenesis of granites. Acta Petrologica Sinica 23, 1217–1238 (in Chinese with English abstract).
Wu, F.Y., Li, X.H., Zheng, Y.F., Gao, S., 2007b. Lu-Hf isotopic systematics and their applications in petrology. Acta Petrologica Sinica 23, 185–220 (in Chinese with English abstract).
Wu, F.Y., Yang, Y.H., Xie, L.W., Yang, J.H., Xu, P., 2006a. Hf isotopic compositions of the standard zircons and baddeleyites used in U-Pb geochronology. Chem. Geol. 234, 105–126.
Wu, R.X., Zheng, Y.F., Wu, Y.B., Zhao, Z.F., Zhang, S.B., Liu, X., Wu, F.Y., 2006b. Reworking of juvenile crust: element and isotope evidence from Neoproterozoic granodiorite in South China. Precambr. Res. 146, 179–212.
Xie, L.W., Zhang, Y.B., Zhang, H.H., Sun, J.F., Wu, F.Y., 2008. In situ simultaneous determination of trace elements, U-Pb and Lu-Hf isotopes in zircon and baddeleyite. Chin. Sci. Bull. 53, 1565–1573.
Xie, Y.C., Lu, J.J., Yang, P., Ma, D.S., Xu, Z.W., Zhang, R.Q., Cai, Y., Ding, T., 2015. S, Pb, C and O isotopic characteristics and sources of metallogenic materials of Baoshan Pb-Zn deposit, southern Hunan province. Mineral Deposits 34, 333–351 (in Chinese with English abstract).
Xie, Y.C., Lu, J.J., Ma, D.S., Zhang, R.Q., Gao, J.F., Yao, Y., 2013. Origin of granodiorite porphyry and mafic microgranular enclave in the Baoshan Pb-Zn polymetallic deposit, southern Hunan Province: Zircon U-Pb chronological, geochemical and Sr-Nd-Hf isotopic constraints. Acta Petrologica Sinica 29, 4186–4214 (in Chinese with English abstract).
Xu, J., Zheng, Y.Y., Sun, X., Li, X.F., Mao, G.Z., 2018. Genesis of the Yaguila Pb-Zn-Ag-Mo skarn deposit in Tibet: Insights from geochronology, geochemistry, and fluid inclusions. J. Asian Earth Sci. 172, 83–100.
Xu, X.S., O'Reilly, S.Y., Griffin, W.L., Wang, X.L., Pearson, N.J., He, Z.Y., 2007. The crust of Cathaysia: age, assembly and reworking of two terranes. Precambr. Res. 158, 51–78.
Yang, J.H., Peng, J.T., Zheng, Y.F., Hu, R.Z., Bi, X.W., Zhao, J.H., Huang, J.H., Zhang, B.L., 2016. Petrogenesis of the Mesozoic Shuikoushan peraluminous I-type granodioritic intrusion in Hunan Province, South China: Middle-lower crustal reworking in an extensional tectonic setting. J. Asian Earth Sci. 123, 224–242.
Yang, Z.Y., Wang, Q., Zhang, C.F., Yang, J.H., Ma, L., Wang, J., Sun, P., Qi, Y., 2019. Cretaceous (~100 Ma) high-silica granites in the Gajin area, Central Tibet: Petrogenesis and implications for collision between the Lhasa and Qiangtang Terranes. Lithos 324, 402–417.
Yu, J.H., Wang, L.J., Wang, X.L., Qiu, J.S., Zhao, L., 2007. Geochemistry and geochronology of the Fucheng Complex in the southeastern Jiangxi province, China. Acta Petrologica Sinica 23, 1441–1456 (in Chinese with English abstract).
Yuan, Z.X., Wu, L.S., 1991. The Sm-Nd, Rb-Sr isotopic age-dating of Mayuan Group in northern Fujian. Acta Petrological et Mineralogica 10, 127–132 (in Chinese with English abstract).
Zhao, G.C., 2015. Jiangnan Orogen in South China: developing from divergent double subduction. Gondwana Res. 27, 1173–1180.
Zhao, J.X., Li, G.M., Evans, N.J., Qin, K.Z., Li, J.X., Zhang, X.N., 2016. Petrogenesis of Paleocene-Eocene porphyry deposit-related granitic rocks in the Yaguila-Sharang ore district, central Lhasa terrane, Tibet. J. Asian Earth Sci. 129, 38–53.
Zhao, K.D., Jiang, S.Y., Yang, S.Y., Dai, B.Z., Lu, J.J., 2012. Mineral chemistry, trace elements and Sr-Nd-Hf isotope geochemistry and petrogenesis of Cailing and Furong granites and mafic enclaves from the Qitianling batholith in the Shi-Hang zone, South China. Gondwana Res. 22, 310–324.
Zhao, P.L., Yuan, S.D., Mao, J.W., Santosh, M., Zhang, D.L., 2017. Zircon U-Pb and Hf–O isotopes trace the architecture of polymetallic deposits: A case study of the Jurassic ore-forming porphyries in the Qin-Hang metallogenic belt, China. Lithos 292, 132–145.
Zhao, Z.F., Zheng, Y.F., Wei, C.S., Wu, Y.B., 2007. Post-collisional granitoids from the Dabie orogen in China: Zircon U-Pb age, element and O isotope evidence for recycling of subducted continental crust. Lithos 93, 248–272.
Zheng, Y.F., Zhang, S.B., Zhao, Z.F., Wu, Y.B., Li, X., Li, Z., Wu, F.Y., 2007. Contrasting zircon Hf and O isotopes in the two episodes of Neoproterozoic granitoids in South China: implications for growth and reworking of continental crust. Lithos 96, 127–150.
Zhou, X.M., Sun, T., Shen, W.Z., Shu, L.S., Niu, Y.L., 2006. Petrogenesis of Mesozoic granitoids and volcanic rocks in South China: a response to tectonic evolution. Episodes 29, 26–33.
Zhu, J.C., Xie, C.F., Zhang, P.H., Yang, C., Gu, C.Y., 2005. Niumiao and Tong'an intrusive bodies of NE Guangxi: Petrology, zircon SHRIMP U-Pb geochronology and geochemistry. Acta Petrologica Sinica 21, 665–676 (in Chinese with English abstract).
Zhu, J.C., Zhang, P.H., Xie, C.F., Zhang, H., Yang, C., 2006. The Huashan-Guposhan A-type Granitoid belt in the western part of the Nanling Mountains: Petrology, Geochemistry and Genetic Interpretations. Acta Geol. Sin. 80, 529–542 (in Chinese with English abstract).
Zuo, C.H., Lu, R., Zhao, Z.X., Xu, Z.W., Lu, J.J., Wang, R.C., Chen, J.Q., 2014a. LA-ICP-MS zircon U-Pb age, and Hf isotope of granodiorite in the Shuikoushan deposit, Changning, Hunan Province. Geol. Rev. 60, 811–823 (in Chinese with English abstract).
Zuo, C.H., Xu, Z.W., Lu, X.C., Zhao, Z.X., Chen, W., Wang, H., Lu, J.J., 2014b. Petrogenesis of the late Jurassic Laomengshan rhyodacite (Southeast China): constraints from zircon U-Pb dating, geochemistry and Sr–Nd–Pb–Hf isotopes. Int. Geol. Rev. 56, 1964–1983.